Manuscript Details

Manuscript number	CATTOD_2018_892_R1
Title	Influences of Na+ co-cation on the structure and performance of Cu/SSZ-13 selective catalytic reduction catalysts
Article type	Research paper

Abstract

A series of Cu/H-SSZ-13 and Cu/Na-SSZ-13 catalysts are synthesized, degreened and hydrothermally aged for use in the standard NH3-SCR reaction. Surface area/pore volume and XRD analyses are used to probe the textural properties of the catalysts. H2-TPR and EPR are used to quantitatively describe the various Cu species. NH3-SCR is carried out at a lower space velocity to probe the light-off behavior, and a higher space velocity to generate data for kinetic analysis. Na+ co-cation addition is found to promote turnover rates of isolated Cu-ions at low reaction temperatures. However, as Cu loadings increase, this promoting effect is compromised by decreases in Cu exchange capacity and hydrothermal stability of the Cu/Na-SSZ-13 catalysts.

Keywords	Cu/SSZ-13; SCR; catalyst additive; sodium; EPR;TPR.

Corresponding Author	Feng Gao
Corresponding Author's Institution	Pacific Northwest National Laboratory
Order of Authors	Yanran Cui, Yilin Wang, Eric Walter, Janos Szanyi, Yong Wang, Feng Gao

Submission Files Included in this PDF

File Name [File Type]

cover letter_revision.docx [Cover Letter]

Responses to reviewer comments.docx [Response to Reviewers]

Highlights.docx [Highlights]

Graphical Abstract.docx [Graphical Abstract]

Na cocation effect paper_revision.docx [Manuscript File]

Na cocation effect SI_revision.docx [Supporting File]

To view all the submission files, including those not included in the PDF, click on the manuscript title on your EVISE Homepage, then click 'Download zip file'.

Research Data Related to this Submission

There are no linked research data sets for this submission. The following reason is given:
The authors are unable or have chosen not to specify which data has been used

Highlights

1) Na^+ addition promotes low temperature turnover rates of Cu/SSZ-13 catalysts.

2) Na^+ addition adversely influences dispersion of isolated Cu-ions.

3) Na^+ addition adversely influences catalyst hydrothermal stability at high Cu loadings.

4) Co-cation addition to Cu/SSZ-13 can be used in practical SCR catalysts, however care must be taken to control the extents.

5) Discussions on quantification of isolated Cu-ions with EPR and H_2-TPR.

Graphical Abstract

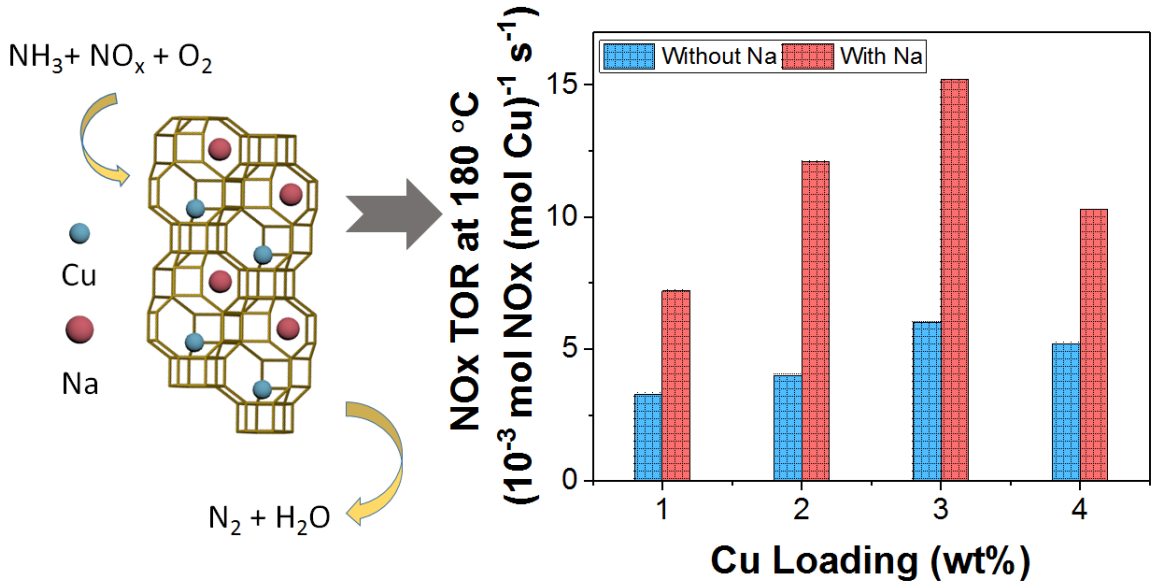

Influences of Na^+ co-cation on the structure and performance of Cu/SSZ-13 selective catalytic reduction catalysts

Yanran Cui, Yilin Wang, Eric D. Walter, János Szanyi, Yong Wang, Feng Gao*

Institute for Integrated Catalysis, Pacific Northwest National Laboratory, P.O. Box 999, Richland, WA 99354, United States

Abstract

A series of Cu/H-SSZ-13 and Cu/Na-SSZ-13 catalysts are synthesized, degreened and hydrothermally aged for use in the standard NH_3-SCR reaction. Surface area/pore volume and XRD analyses are used to probe the textural properties of the catalysts. H_2-TPR and EPR are used to quantitatively describe the various Cu species. NH_3-SCR is carried out at a lower space velocity to probe the light-off behavior, and a higher space velocity to generate data for kinetic analysis. Na^+ co-cation addition is found to promote turnover rates of isolated Cu-ions at low reaction temperatures. However, as Cu loadings increase, this promoting effect is compromised by decreases in Cu exchange capacity and hydrothermal stability of the Cu/Na-SSZ-13 catalysts.

Keywords:

*Corresponding author – email address: feng.gao@pnnl.gov (F. Gao).

1. Introduction

The selective catalytic reduction of NO_x with ammonia (NH_3-SCR) is an important reaction for diesel engine exhaust abatement [1-4]. Cu/SSZ-13 has attracted the most attention in recent years as a SCR catalyst for two reasons: (1) its great catalytic performance in terms of high activity, selectivity and superior stability; (2) its structural simplicity (in comparison to other Cu/zeolites) in enabling fundamental research [5-9]. With extensive research efforts for more than a decade, researchers are now having a very good understanding about this catalytic reaction, including but not limited to the nature of the active sites and reaction mechanism. It is now generally agreed that Cu/SSZ-13 contains two active sites for SCR, $[Cu(OH)]^+$-Z and Cu^{2+}-2Z, where the former is charge-balanced by a single framework negative charge (Z), and the latter balanced by a pair of negative charges (2Z) [6, 10, 11]. While both sites almost equally catalyze SCR, they have very different (hydrothermal) stabilities. Cu^{2+}-2Z is thermodynamically more stable than $[Cu(OH)]^+$-Z [12]. It has been suggested that $[Cu(OH)]^+$-Z only populates upon Cu^{2+}-2Z saturation, as one would expect, based on such a thermodynamic ground [13]. However a few recent studies demonstrated that $[Cu(OH)]^+$-Z can populate prior to Cu^{2+}-2Z saturation, believed to be caused by kinetic stabilization effects [7, 11, 14, 15]. In a recent study, Song et al. [11] utilized electron paramagnetic resonance (EPR) to quantify different Cu moieties in Cu/SSZ-13, and discovered that $[Cu(OH)]^+$-Z converts to unwanted CuO_x clusters during hydrothermal aging. CuO_x clusters play two detrimental roles: (1) they lower SCR selectivities by catalyzing the side, NH_3 oxidation reactions; and (2) they actively promote degradation of the SSZ-13 supports during aging [11].

From the studies shown above, it can be concluded that both Cu content and positioning play important roles in SCR performance and long-term stability of Cu/SSZ-13 catalysts. Catalyst optimization efforts, therefore, should consider a number of factors including Cu/Al and Si/Al

ratios, Al distribution, catalyst treatments (e.g., degreening), etc., since these all influence Cu positioning [8]. Cu positioning can also be influenced by other species unintentionally introduced into the SCR catalysts during application, i.e., Zn and P from engine oil, minerals within urea solution, and noble metals from the upper stream emission abatement component (e.g., diesel oxidation catalyst, DOC) [16]. Sodium is another common element found in Cu/SSZ-13 catalysts for reasons as follows: SSZ-13 synthesis typically requires a strong basic environment provided by NaOH; incomplete exchange between Na/SSZ-13 and NH_4^+ solutions, typically employed to remove Na prior to Cu-exchange, leads to coexistence of Na^+ and Cu^{2+} in the final products. In a recent study, Gao et al. [17] demonstrated that the presence of certain amounts of Na^+ (and other alkali and alkaline earth cations) is beneficial to both low temperature NO_x conversion and hydrothermal stability of low-Cu loaded Cu/SSZ-13. A recent patent application by Johnson Matthey, Inc. also demonstrated stability enhancement roles of a number of co-cation additives (Na^+ included) [18]. From these prior investigations, we can at least suggest three roles that Na^+ co-cations play: (1) competing with Cu-ions for catalytic exchange sites; (2) neutralizing Brønsted acid sites thus preventing dealumination during hydrothermal aging; (3) providing NH_3 adsorption function as Lewis acids. These roles have not yet been thoroughly investigated. In this work, a series of Cu/SSZ-13 catalysts with and without Na^+ co-cations have been prepared and systematically investigated in both degreened and hydrothermally aged forms. Isolated Cu sites, i.e., active centers in this catalyst, were quantified using EPR. The influences of Cu content on catalyst structure, SCR activity and thermal stability were investigated to elucidate the multiple roles Na^+ co-cations play.

2. Material and Methods

2.1 Catalyst Preparation

Na-SSZ-13 with Si/Al = 9 was hydrothermally synthesized in house [19]. Typically, 0.8 g NaOH (Sigma Aldrich, ≥ 99%) was dissolved in 50 ml deionized water. 1.2 g $Al(OH)_3$ (Sigma Aldrich, containing ~54wt% Al_2O_3) was added and stirred until completely dissolved. Then 17.1 g TMAda-OH (Sachem Inc., containing ~25% trimethyladamantylammonium hydroxide) was added as the structure directing agent (SDA). 24.0 g LUDOX HS-30 colloidal silica (Sigma Aldrich, 30 wt% suspension in H_2O) was added slowly to the solution until a uniform white gel was formed. The stoichiometric composition of the gel was as follows: 40 SDA : 10 NaOH : 2.9 Al_2O_3 : 60 SiO_2 : 1860 H_2O. The gel was sealed in a 125 ml Teflon-lined stainless steel autoclave containing a magnetic stir bar. The autoclave was placed in a sand bath on top of a hot plate stirrer. The gel was continuously stirred at 160 °C for 4 days at 400 rpm. Note that gel stirring is critical for the synthesis of SSZ-13 materials with narrow particle size distributions [20]. The final solid product was separated from the solution by centrifugation and washed three times with deionized water. It was then dried under a nitrogen flow at 60 °C overnight, and calcined at 550 °C for 5 h in static air to burn the SDA. The thus prepared Na-SSZ-13 substrate contains 1.50 wt% of sodium, determined with inductively coupled plasma atomic emission spectroscopy (ICP-AES), performed at Galbraith Laboratories (Knoxville, TN, U.S.A.). A portion of the Na-SSZ-13 substrate was converted to NH_4-SSZ-13 by exchange with NH_4NO_3 solutions. Typically, 10 g of Na-SSZ-13 was mixed with 8 g of NH_4NO_3 (Sigma Aldrich, ≥ 99%) and 100 ml deionized water. The mixture was stirred at 80 °C for 2 h. The product was centrifuged and washed with deionized water for a few times. To ensure complete Na^+ removal, the process was repeated twice. The solid NH_4-SSZ-13 material was dried under a nitrogen flow at 60 °C overnight. Both the Na-SSZ-13 and NH_4-SSZ-13 substrates were stored at ambient conditions for further use.

Cu ion-exchange was carried out using the Na-SSZ-13 and NH_4-SSZ-13 substrates and $Cu(NO_3)_2$. Various amounts of $Cu(NO_3)_2 \cdot 2.5H_2O$ (Sigma Aldrich, ≥ 99%) was first dissolved in 100 ml water. 1 g of Na-SSZ-13 or NH_4-SSZ-13 was then added to the solution. Exchange was carried out at 80 °C for 2 h under stirring. The temperature was then raised to ~150 °C to evaporate water to obtain the dry powder, still under continuous stirring. The solid powders were then calcined in static air at 550 °C for 5 h. In this way, two series of samples were prepared: a Cu/H-SSZ-13 series that contain Cu loadings of 1-5 wt%, and a Cu/Na-SSZ-13 series that contain Cu loadings of 1-4 wt% (note again that this series contain 1.5 wt% of Na in each sample). A portion of the freshly prepared Cu/H-SSZ-13 and Cu/Na-SSZ-13 catalysts were degreened (abbreviated as DG) at 700 °C for 4 h in flowing air containing 10% H_2O. Some fresh catalysts were also hydrothermally aged (denoted as HTA) at 800 °C for 16 h under the same gas flow. Characterizations and reaction testing were mainly conducted on the DG and HTA catalysts. Note that all of the catalysts studied here were prepared using the same batch of parent SSZ-13 material to minimize potential zeolite particle size/shape effects on catalysis.

2.2 Standard NH_3-SCR and NH_3 oxidation reaction tests

The standard NH_3-SCR ($4NO + 4NH_3 + O_2 = 4N_2 + 6H_2O$) "light-off" curves were measured in a plug-flow reactor system described elsewhere [19, 21]. 120 mg of sieved catalyst (60-80 mesh) was loaded in a 1cm OD quartz reactor and placed in an electric tube furnace. The composition of the gas feed was 360 ppm NH_3, 360 ppm NO, 14% O_2, 2.5% H_2O and balanced N_2. The total flow rate was 300 ml/min and the gas hourly space velocity (GHSV) was estimated to be ~100, 000 h^{-1}. Concentrations of reactants and products were measured by an online MKS MultiGas™ 2030 FTIR gas analyzer with the gas cell maintained at 191 °C. The NO_x ($NO + NO_2$) conversions were measured at temperatures decreasing stepwise from 550 to 200 °C with intervals of 50 or 20 °C.

At each temperature, the measurement was maintained at least for 1 hour in order for the reaction to reach steady-state. NO_x conversions were calculated using the following equation:

$$NO_x\ conversion = \frac{(NO_x)_{inlet} - (NO_x)_{outlet}}{(NO_x)_{inlet}} \times 100\%$$

The NH_3 oxidation reaction ($4NH_3 + 3O_2 = 2N_2 + 6H_2O$) tests were carried out after the standard SCR tests on the same catalysts at the same space velocities and the same ways of temperature ramping. The gas feed contained 380 ppm NH_3, 14% O_2 and balanced N_2. The NH_3 conversions were calculated as follows:

$$NH_3\ conversion = \frac{(NH_3)_{inlet} - (NH_3)_{outlet}}{(NH_3)_{inlet}} \times 100\%$$

To obtain SCR kinetics parameters, e.g., apparent activation energies using the Arrhenius equation, steady-state measurements were also carried out under kinetic control. In this case, 60 mg catalyst was typically used and a higher flow rate of 1, 000 ml/min was chosen, resulting in an estimated GHSV of 667, 000 h^{-1}. The reaction temperatures were varied from 180 to 100 °C with 10 °C intervals. The absence of mass and heat transfer limitations was tested using the Koros-Nowak criterion [21, 22].

2.3 Characterizations

BET surface areas and micropore volumes of the catalysts were measured with a Quantachrome Autosorb-6 analyzer with liquid N_2 adsorption. The catalysts were degassed under vacuum overnight at 250 °C prior to analysis. Powder X-ray diffraction (XRD) measurements were performed on a Philips PW3040/00 X'Pert powder X-ray diffractometer with Cu Kα

radiation (λ = 1.5406 Å). Data were collected with 2θ ranging from 5 to 50° using a step size of 0.02°.

The isolated Cu(II) contents of the catalysts were quantified by EPR. Typically, ~10 mg of ambient hydrated catalyst was loaded in the quartz EPR tube and continuous scan of the sample was performed at 125 K. The acquired spectra were double-integrated to obtain signal areas, which are proportional to EPR active isolated Cu(II) contents. To quantify these, a series of standard solutions with different isolated Cu(II) concentrations were prepared by dissolving $Cu(NO_3)_2 \cdot 2.5H_2O$ and imidazole (Sigma Aldrich, 99%) in ethylene glycol (Sigma Aldrich, 99.8%). Imidazole was used here to coordinate with Cu(II) ions to prevent formation of EPR silent Cu dimers. The linear calibration curve generated using the integral areas and Cu contents of the standard solutions was then used for quantification of isolated Cu(II) in the catalysts.

The H_2 temperature programmed reduction (H_2-TPR) experiment was performed on a Micromeritics AutoChem 2920 apparatus. ~100 mg of catalyst was used for each experiment. The catalyst was first purged with N_2 at room temperature (note that a dehydration pretreatment was not performed to avoid autoreduction of $[Cu(OH)]^+$-Z [19]). Then 10% H_2/Ar was flowed through the quartz sample holder at a total flow rate of 50 ml/min. The temperature was ramped from ambient to 1000 °C with a ramping rate of 10 °C/min, and maintained at 1000 °C for 15 mins before cooling down. The obtained TPR curves were integrated and normalized by sample weight. CuO (Sigma Aldrich, 99.9%) reduction with the same procedure was used as the quantification standard.

NH_3 temperature programmed desorption (NH_3-TPD) was performed using the SCR test unit. ~120 mg catalyst was loaded in the reactor and calcined at 500 °C for 1 hour under a 300 ml/min N_2 flow. The sample was then cooled down to 100 °C and saturated with 360 ppm NH_3 balanced

with N_2 (total flow rate 300 ml/min) until the outlet NH_3 concentration maintained invariant for 30 min. The catalyst was then purged with 300 ml/min N_2 flow for 2 h at 100 °C to remove weakly adsorbed species. Next, the sample was heated from 100 to 700 °C with a ramping rate of 10 °C/min under 300 ml/min N_2 flow, and was kept at 700 °C for 30 min to ensure complete NH_3 desorption before cooling down. The desorbed NH_3 was monitored with the MKS MultiGasTM 2030 FTIR gas analyzer described above.

3. Results

3.1 Textural properties of the catalysts

Textural properties of the catalysts are first studied with N_2 adsorption. **Figure S1** presents N_2 adsorption-desorption isotherms of the Na-SSZ-13 and NH_4-SSZ-13 substrates. These are typical type I isotherms consistent with the micropore nature of these materials. Small gaps between adsorption and desorption curves indicate the presence of small amounts of mesopores due to stacking of the primary particles. Surface areas (BET method) and micropore volumes (t-plot method) of the Cu/H-SSZ-13 and Cu/Na-SSZ-13 DG and HTA samples are tabulated in **Table 1**. The DG catalysts have surface areas ≥ 500 m^2/g and micropore volumes ≥ 0.25 cm^3/g, very similar to those of the freshly prepared SSZ-13 substrate (550 m^2/g and 0.25 cm^3/g, respectively). This demonstrates that the degreening treatment causes only minor structural damages irrespective of catalyst compositions. Following the much more severe HTA treatment, however, a strong Cu loading dependence is found: surface areas and pore volumes largely maintain in samples below a threshold Cu loading, but decrease dramatically in samples with Cu contents above that threshold. For the Cu/H-SSZ-13 series of samples, the threshold Cu loading is found at ~3.5wt%, which drops to ~1.5wt% for the Cu/Na-SSZ-13 series of samples. At the same Cu loadings (> 1.5wt%),

the HTA Cu/Na-SSZ-13 samples invariably have lower surface areas and micropore volumes in comparison to their HTA Cu/H-SSZ-13 counterparts, suggesting an "apparent" structural destructive role for Na^+. This will be discussed further below. The textural properties of the catalysts were also probed with XRD. **Figure S2** of the Supporting Information (SI) presents the XRD patterns of Cu/H-SSZ-13 and Cu/Na-SSZ-13 DG and HTA samples. To quantitatively describe these patterns, relative crystallinities of these samples were calculated (detailed in SI). **Figure S3** presents relative crystallinities of the DG and HTA samples as a function of Cu loading. These relative crystallinities are fully consistent with data shown in **Table 1**, again demonstrating the strong aging temperature and Cu loading effects on structural integrity of these catalysts.

3.2 Characterizations of Cu species

Figure 1 (a) and (b) shows the H_2-TPR results of selected DG and HTA Cu/H-SSZ-13 samples, respectively, where two widely separated reduction states exist: reduction between ~150 and 500 °C, and reduction above ~700 °C. The high-temperature state is due entirely to reduction of isolated Cu^+ ions to Cu^0 ($Cu^+ + ½\ H_2 = Cu^0 + H^+$) [23]. The low-temperature one contains a few possible contributions: (1) Cu^{2+}-2Z and $[Cu(OH)]^+$-Z reduction to Cu^+-Z ($Cu^{2+} + ½\ H_2 = Cu^+ + H^+$; $[Cu(OH)]^+ + ½\ H_2 = Cu^+ + H_2O$) [19]; (2) reduction of CuO_x clusters or particles to Cu^0 ($CuO + H_2 = Cu^0 + H_2O$) [24]; and (3) reduction of copper aluminate-like species, which are sometimes present in samples undergone harsh hydrothermal aging (not expected in our DG samples), to Cu^0 ($CuAl_2O_4 + H_2 = Cu^0 + H_2O + Al_2O_3$) [25]. For the DG Cu/H-SSZ-13 samples (**Figure 1(a)**), reduction at ~210 °C can be attributed to $[Cu(OH)]^+$-Z reduction to Cu^+-Z, and reduction at ~350 °C can be attributed to Cu^{2+}-2Z reduction to Cu^+-Z. Shoulder peaks at ~230 °C are due to reduction of CuO_x clusters or particles. For samples after HTA at 800 °C (**Figure 1(b)**), the low-temperature reduction becomes more complex. The most obvious change in comparison to the DG samples is

the decrease of the reduction at ~210 °C, indicative of $[Cu(OH)]^+$-Z conversion to other species [11]. However, there are also changes that are not readily understood. For example, at relatively high Cu loadings, a new reduction state at ~300 °C develops. The origin of this state will be further discussed below. Because of this complexity, no effort was exerted to deconvolute and quantify different low temperature peaks. Instead, overall H_2 consumptions below 500 °C and above 700 °C were integrated, and the results are tabulated in **Table S1**. Based on the reduction reactions shown above, two reasonable assumptions are made here: (1) high-temperature H_2 consumptions represent isolated Cu(II) ions; and (2) differences between low- and high-temperature H_2 consumption represents multinuclear CuO_x species (including $CuAl_2O_4$ in the HTA samples). On the basis of these assumptions, the amounts of SCR active isolated Cu(II) ions (i.e., the sum of $[Cu(OH)]^+$-Z and Cu^{2+}-2Z) and SCR inert species can be readily quantified.

Figure 2 (a) and (b) presents the H_2-TPR results of selected Cu/Na-SSZ-13 DG and HTA samples. In comparison to H_2-TPR results of degreened Cu/H-SSZ-13 shown in Figure 1(a), degreened Cu/Na-SSZ-13 displays clear differences: (1) both of the $[Cu(OH)]^+$-Z (~210 °C) and CuO_x (~230 °C) reduction peaks shift to lower temperatures and become narrower, suggesting a promoting role of Na^+ in assisting their reduction; (2) Cu^{2+}-2Z reduction (~350 °C) becomes much weaker and less resolved, suggesting that Na^+ lowers Cu^{2+}-2Z formation during ion-exchange; (3) the high-temperature reduction state becomes much weaker, or even barely detectable in high Cu-loaded samples. This either indicates that the effect for Na^+ in promoting Cu reduction is so strong that the majority of isolated Cu^+ ions are reduced below ~500 °C, or the presence of Na^+ lowers formation of isolated Cu(II) ions as suggested immediately above. After hydrothermal aging at 800 °C (Figure 2(b)), $[Cu(OH)]^+$-Z consumption is again seen decreased as indicated by the declined intensity of the ~210 °C peaks. Also the low-temperature state broadens considerably for

all samples, due primarily to merging of the low-temperature peak into the new reduction state at ~300 °C. These changes qualitatively resemble those found for the HTA Cu/H-SSZ-13 samples. In the high temperature region, Cu^{+} reduction is again very weak, and appears to shift somewhat to lower temperatures. Low- and high-temperate H_2 consumptions were quantified and the results are shown in **Table S2**. Because of their low signal intensities, the high-temperature H_2 consumption results, particularly for the high Cu-loaded samples, are not considered very reliable. In any case, it can still be safely concluded that the Cu/Na-SSZ-13 samples contain much less isolated Cu(II) but much more multinuclear CuO_x species as compared to their Cu/H-SSZ-13 counterparts at the same Cu loadings.

In order to more accurately quantify isolated Cu(II) ions in the catalysts, EPR was utilized next. We have demonstrated previously that both hydrated $[Cu(OH)]^{+}$-Z and Cu^{2+}-2Z are EPR active [11]. Upon dehydration, Cu^{2+}-2Z remains EPR active but $[Cu(OH)]^{+}$-Z will either become EPR silent itself because of a pseudo Jahn-Teller effect [26], or convert to other EPR silent species, e.g., Cu(I) or oligomeric clusters [11]. Therefore, to quantify all of the SCR active Cu(II) ions, fully hydrated samples are needed. Moreover, measurements should be performed at cryogenic temperatures to prevent signal loss due to dipolar interactions between mobile Cu(II) ions. As shown in **Figure 3**, the EPR active Cu(II) content increases almost linearly with increasing total Cu loading for the DG Cu/H-SSZ-13 samples, and saturates at ~2.5 wt% when total Cu loadings reach ~3.5 wt% and higher. In the HTA samples, the EPR active Cu(II) contents remain largely unchanged at total Cu loadings ≤ 3.5 wt%. At higher Cu loadings, EPR active Cu(II) contents become lower than the corresponding DG samples, likely due to structural degradation of the high Cu-loaded HTA samples. In contrast, EPR active Cu(II) contents in the DG and HTA Cu/Na-SSZ-13 samples are much lower and maintain largely invariant among samples. From both H_2-TPR and

EPR analyses, it is readily concluded that in comparison to NH_4-SSZ-13, Cu(II) ion exchange capacity for Na-SSZ-13 is clearly lower.

Even though very powerful, EPR still has one disadvantage quantifying SCR active Cu species. $CuAl_2O_4$-like species, which forms under harsh hydrothermal aging conditions [25], also contain EPR active Cu(II) sites that are not readily distinguishable from Cu^{2+}-2Z and $[Cu(OH)]^+$-Z sites. For example, the HTA Cu/Na-SSZ-13 sample with 4.0 wt% Cu loading experienced dramatic structural damage during aging (Table 1), yet it contains similar EPR active Cu as other Cu/Na-SSZ-13 samples. It is expected that substantial amount of EPR active Cu(II) in this samples is contributed by $CuAl_2O_4$-like species. However for all of the DG samples and other HTA samples without apparent structural degradation, EPR active contributions from $CuAl_2O_4$-like species are believed to be negligible.

3.3 Standard NH_3-SCR reaction tests

Figure 4 presents standard NH_3-SCR NO_x conversions as a function of temperature for selected degreened catalysts. Low-temperature (≤ 200 °C) NO_x conversion follows an interesting dependence on Cu loading as follows: at a low Cu loading of 1.0 wt%, Cu/Na-SSZ-13 outperforms Cu/H-SSZ-13; at an intermediate Cu loading of 2.0 wt%, the two catalysts show similar performance while at a high Cu loading of 3.0 wt%, Cu/H-SSZ-13 outperforms Cu/Na-SSZ-13. In the high temperature regime (> 350 °C), Cu/Na-SSZ-13 samples with 2.0 and 3.0 wt% Cu loadings display very poor SCR selectivities due to the presence of large amounts of CuO_x species, which are active in catalyzing the NH_3 oxidation side reaction at such high temperatures. Note that **Figure 4** only presents results on selected samples. SCR results for degreened catalysts with other Cu loadings, and all of the HTA samples are collectively shown in **Figure S4**. NH_3 oxidation results

for all of the samples are presented in **Figure S5**. These results corroborate data shown in **Figure 4**.

To obtain a better understanding of the interesting Cu loading dependence shown in **Figure 4**, next SCR reactions were conducted on selected Cu/H-SSZ-13 and Cu/Na-SSZ-13 catalysts under kinetic control. Koros-Nowak criterion was utilized to verify the absence of heat and mass transfer limitations in such kinetics measurements; more details can be found in **Figure S5**. NO_x conversions were then converted to turnover rates (TORs) on a molecules of NO_x converted per EPR active Cu(II) site per second basis. Based on these values, a series of Arrhenius plots were obtained, and the results are depicted in **Figure S7**. To facilitate sample comparison, apparent activation energies and TORs at 180 °C are tabulated in **Table 2**.

4. Discussion

Discussion herein is mainly focused on how Na^+ co-cations influence activity, selectivity and hydrothermal stability of Cu/SSZ-13 catalysts. We note at the onset that catalysts used in this study have a single Si/Al ratio of 9 and the Cu/Na-SSZ-13 ones contain a single Na loading of 1.50 wt%. Therefore, conclusions drawn here may not be generally applicable.

We first discuss our catalyst preparation method. Catalysts used in this work were solution ion-exchanged and then followed by a slurry drying step, i.e., a combination of ion-exchange and impregnation. A traditional solution ion-exchange, in contrast, involves washing with d.i. water after exchange to remove chemicals dissolved in the solution phase. The method adopted here has the advantage of precise Cu loading control and especially, allows for the maintenance of the 1.50 wt% Na^+ in each Cu/Na-SSZ-13 catalyst. However, any unexchanged $Cu(NO_3)_2$ will be deposited on the zeolite external surfaces during drying, and eventually converts to CuO during calcination.

The SSZ-13 substrate used in this study has a Si/Al ratio of 9. This translates to ~3.6 Brønsted acid sites in each hexagonal unit cell ($T_{36}O_{72}$) assuming that all Al occupy framework T sites and each Al is associated with one H^+ [27]. Note also that the as-synthesized Na-SSZ-13 contains 1.50 wt% Na, translating to ~1.4 Na^+ ions in each unit cell. Assuming each Cu^{2+} replaces $2H^+$ during exchange, exchange capacities for our NH_4-SSZ-13 and Na-SSZ-13 substrates are ~5.3 wt% and ~3.2 wt% of Cu-ions, respectively. Considering that some exchanged Cu stays as $[Cu(OH)]^+$-Z, the exchange capacities should be even higher. However as shown in **Figure 3**, only ~2.5 wt% and ~0.7 wt% Cu-ions are exchanged into NH_4-SSZ-13 and Na-SSZ-13, corresponding to ~0.85 and ~0.24 Cu-ions per unit cell, respectively. Therefore, it appears likely that under our solution ion-exchange conditions, repulsions between solvated cations preclude the presence of multiple cations in the same Chabazite cage. Regarding Na^+ ions exchanged out of the zeolite pores, these will be balanced by NO_3^- ions in solution, and will be converted to solid $NaNO_3$ depositing on the zeolite external surface during slurry trying, and then to Na_2O during sample calcination. However, since Na_2O is highly basic, and since the SSZ-13 support has sufficient residual Brønsted acid sites, we hypothesize that during calcination, Na_2O will react with H^+ completely to reform Na^+ ions ($Na_2O + 2H^+ = 2Na^+ + H_2O$) that occupy cationic positions. However, since we do not have a very good method for quantifying Na^+ ions inside and outside SSZ-13 pores, this hypothesis cannot be fully confirmed. It is also possible that during the slurry drying and catalyst calcination steps, some exchanged Cu-ions migrate out of the Chabazite pores. Without further evidence, these possibilities can only be speculated about.

Next, quantification of the various Cu-containing species is briefly discussed. For this catalytic system, quantification of the SCR active species, i.e., Cu^{2+}-2Z and $[Cu(OH)]^+$-Z, is of the highest importance. H_2-TPR has been most frequently used to quantify different Cu species in Cu/SSZ-13

and Cu/SAPO-34 SCR catalysts [23, 28-30]. As shown in **Figures 1** and **2**, quantification of different Cu species based on reduction at low temperatures (< 500 °C) is rather challenging due to heavy overlapping of various reduction features. On the other hand, since SSZ-13 is such a highly refractory material, isolated Cu^{+}-Z ions (originated from low-temperature reduction of Cu^{2+}-2Z and $[Cu(OH)]^{+}$-Z) can only be reduced at very high temperatures, accompanying structural collapse of Chabazite [23]. Therefore, high-temperature H_2 consumption may be used to more accurately quantify isolated Cu(II)-ions. We have shown previously that EPR can be used to quantify Cu^{2+}-2Z and $[Cu(OH)]^{+}$-Z, even separately, with high precision [11]. In the present study, isolated Cu(II)-ions are collectively quantified with EPR, thus allowing us to directly compare these two quantification methods. **Figure 5** plots concentrations of EPR active Cu(II)-ions of the DG and HTA Cu/H-SSZ-13 samples versus their high-temperature (> 700 °C) H_2 consumptions measured with H_2-TPR. For most samples, an excellent linear correlation (R-square > 0.98) exists suggesting that both methods are accurate, and therefore reliable for quantification of isolated Cu ions in structurally intact Cu/SSZ-13. **Figure 5** also contains a few data points that are outliners: for HTA samples at high Cu loadings (≥ 4.0 wt%), high-temperature TPR clearly underestimates the amounts of isolated Cu-ions, where the discrepancies are higher with increasing Cu loading. This can be understood from two aspects: (1) these samples are structurally more defective (Table 1) such that some isolated Cu^{+} ions are reduced at much lower temperatures; (2) the formation of $CuAl_2O_4$-like species (which is associated with Chabazite structural degradation) in these samples, which contain EPR active Cu(II), but are fully reduced to Cu^{0} at lower temperatures. In any case, for structurally defective Cu/SSZ-13, EPR is clearly more reliable in quantifying exchanged isolated Cu(II) ions despite the uncertainty in distinguishing these with Cu in $CuAl_2O_4$-like species. For the Cu/Na-SSZ-13 series of samples, since structural degradation

occurs at much lower Cu loadings, and since Na^+ promotes Cu reduction, high-temperature TPR results (**Figure 2**) are barely useful in quantifying isolated Cu(II) ions.

We have established recently that CuO_x clusters generated during hydrothermal aging are primarily responsible for structural degradation of Cu/SSZ-13, where the migration of these clusters create mesopores; and the accumulation of such mesopores causes structure collapse [11]. In the present study, Cu distribution is more complex: besides isolated Cu(II) ions exchanged into zeolite bulk, CuO_x clusters are also present on zeolite external surfaces in the degreened catalysts. It is anticipated that, if these external surface CuO_x clusters maintain intact during hydrothermal aging, they should not adversely influence structural integrity. To verify if this is the case, **Figure 6** presents the BET surface areas of the HTA catalysts versus EPR silent Cu contents (total Cu subtracted by EPR active Cu, containing primarily multinuclear CuO_x sites) of these samples. Samples with $\leq$ 1 wt% EPR silent Cu have surface areas similar to that of the fresh SSZ-13 substrate. However beyond this threshold, both HTA Cu/H-SSZ-13 and Cu/Na-SSZ-13 samples display marked surface area decrease with increasing contents of EPR silent Cu with approximately linear correlations, where samples containing Na^+ degrade faster. These data corroborate our previous finding that CuO_x clusters are responsible for destruction of the Chabazite structure, even though small amounts ($\leq$ 1 wt%) can still be tolerated. The linear correlations between surface area and EPR silent Cu suggest that external surface CuO_x clusters do migrate into zeolite bulk and aggregate structural degradation during aging. Furthermore, Na^+ ions apparently promote this structure degradation. The mechanism for this promotion effect, however, is not clear at this point. One possible explanation is that CuO_x clusters that are positively charged receive repulsions from Na^+ ions, rendering them more mobile (i.e., more destructive). We have shown previously that for low Cu-loaded Cu/SSZ-13 (i.e., in the absence of structure destructive

CuOx clusters), the presence of Na^+ ions stabilizes the Chabazite framework by suppressing dealumination as determined from ^{27}Al NMR [17].

Finally, the promoting effect of Na^+ ions on low-temperature turnover rates of individual Cu(II) ions is discussed. As shown in **Table 2**, degreened Cu/Na-SSZ-13 catalysts show TORs 2-3 times that of the corresponding Cu/H-SSZ-13 catalysts at 180 °C. After hydrothermal aging, the Cu/Na-SSZ-13 catalysts still have TORs higher than Cu/H-SSZ-13 except the one with 4.0 wt% Cu loading which excessively degraded during aging. This Na^+ promoted TOR increase nicely explains the reaction results shown in **Figure 4**: at low Cu loadings, higher NO_x conversions are achieved on Cu/Na-SSZ-13. However, as the Cu loading increases, this promoting effect is compromised by the much lower Cu-ion exchange capacities of Na-SSZ-13 (**Figure 3**).

Low-temperature SCR can be expressed using the following empirical rate equation [19],

$$R_{SCR} = Ae^{-E_a/RT} P_{NO} \theta_{NH_3} \qquad \text{(eq. 1)}$$

where A is the pre-exponential factor, E_a the apparent activation energy and θ_{NH_3} the coverage of reactive forms of NH_3. Note that the presence of Na^+ causes decrease in reduction temperatures of Cu(II) during H_2-TPR (**Figures 1** and **2**). This may suggest that the redox barriers for Cu-ions decrease in the presence of Na^+, possibly explaining the rate enhancement role of Na^+. From the apparent activation energies displayed in **Table 2** , except for the samples with a Cu loading of 1.0 wt% where the low activation energies may be due to a unique Cu(I) oxidation rate-limiting step [31, 32], activation energies for the higher Cu-loaded samples do not appear to display a dependence on Na^+. In order to probe whether NH_3 storage plays a role, NH_3-TPD was conducted. **Figure 7** presents NH_3-TPD results of selected degreened Cu/H-SSZ-13 and Cu/Na-SSZ-13 catalysts. Briefly, low temperatures (~200 °C) signals are attributed to NH_3 desorption from Lewis

acid sites, i.e., extraframework Al (EFAl) and Na^+; features at ~300 °C are due to desorption from Cu-ions; and the higher temperature signals are assigned to desorption from Brønsted acid sites [17]. NH_3-TPD results of the corresponding HTA catalysts and the calculated total NH_3 desorption yields are presented in **Figure S8** and **Figure S9**. Clearly total NH_3 desorption yields poorly represent θ_{NH_3}in eq. 1. Clearly, not all of the adsorbed NH_3 is equally reactive for the SCR reaction. It has been reported that the weakly adsorbed NH_3 on Lewis acid sites are significantly more active than the NH_3 adsorbed on Brønsted acid sites. NH_3 on Brønsted acid sites form stable NH_4^+, which does not participate in the reaction pathway directly, but serves as NH_3 reservoir to provide NH_3 for Cu sites [33]. One likely explanation for the activity difference is that relatively weakly adsorbed NH_3 is more reactive and thus represents θ_{NH_3} much better. Indeed, the Cu/Na-SSZ-13 catalysts have stronger NH_3 desorption than Cu/H-SSZ-13 at lower temperatures (**Figure 7**). In other words, Cu/Na-SSZ-13 catalysts contain larger reservoirs of more reactive NH_3 that is beneficial to low-temperature NO_x conversion. This enhancement can also be understood from the fact that the larger reactive NH_3 reservoirs effectively induce an increase of the pre-exponential factor A of eq. 1. However, the applicability of this beneficial effect to industrial SCR catalysts is questionable based on the results of this study since Na^+ ions also display unwanted features: they decrease ion-exchange capacity of the SSZ-13 substrate (**Figure 3**), and they deteriorate hydrothermal stability of the catalysts (**Figure 6**). Still, these conclusions are based on results obtained using catalysts with Si/Al = 9 and a single Na loading of 1.50 wt%. For SSZ-13 materials with lower Si/Al ratios (i.e., higher ion-exchange capacities), it remains an open question whether or not the addition of certain amounts of Na^+ co-cations leads to catalysts with improved catalytic performance and long-term stability.

Conclusions

A series of Cu/H-SSZ-13 and Cu/Na-SSZ-13 catalysts were synthesized for the standard NH_3-SCR reaction. The presence of Na^+ co-cations causes a few effects that are important to SCR. First, their presence lowers Cu-ion exchange capacity, likely because of repulsions between Cu(II)-ions and Na^+ cations during ion-exchange. Because of this, Cu/H-SSZ-13 catalysts contain higher amounts of isolated Cu-ions, and lower amounts of CuO_x clusters, in comparison to Cu/Na-SSZ-13 catalysts with the same total Cu loadings. The presence of CuO_x clusters, beyond a threshold of ~1.0 wt%, is detrimental to hydrothermal stability of the catalysts. The presence of Na^+ aggravates this adverse effect. However, Na^+ co-cations provide a beneficial effect of enhancing low-temperature turnover rates of isolated Cu-ion active sites. This effect is believed to be caused by NH_3 adsorption on Na^+ as a reservoir for reactive NH_3. However, this beneficial effect only leads to catalyst performance enhancement at relatively low Cu loadings ($\leq$ 1.5 wt%). At higher Cu loadings, this effect is overwhelmed by the detrimental effects.

Acknowledgement

The authors gratefully acknowledge the US Department of Energy (DOE), Energy Efficiency and Renewable Energy, Vehicle Technologies Office for the support of this work. The research described in this paper was performed in the Environmental Molecular Sciences Laboratory (EMSL), a national scientific user facility sponsored by the DOE's Office of Biological and Environmental Research and located at Pacific Northwest National Laboratory (PNNL). PNNL is operated for the US DOE by Battelle. The authors gratefully appreciate fruitful discussions with CRADA collaborators Craig Dimaggio, Kiran Premchand, Vencon Easterling and Mike Zammit from Fiat Chrysler Automobiles (FCA).

References

[1] T.V. Johnson, Review of diesel emissions and control, Int J Engine Res, 10 (2009) 275-285.
[2] K. Kamasamudram, N.W. Currier, X. Chen, A. Yezerets, Overview of the practically important behaviors of zeolite-based urea-SCR catalysts, using compact experimental protocol, Catal Today, 151 (2010) 212-222.

[3] P. Forzatti, L. Lietti, I. Nova, E. Tronconi, Diesel NO(x) aftertreatment catalytic technologies: Analogies in LNT and SCR catalytic chemistry, Catal Today, 151 (2010) 202-211.
[4] S. Brandenberger, O. Krocher, A. Tissler, R. Althoff, The State of the Art in Selective Catalytic Reduction of NOx by Ammonia Using Metal-Exchanged Zeolite Catalysts, Catal Rev, 50 (2008) 492-531.
[5] F. Gao, J.H. Kwak, J. Szanyi, C.H.F. Peden, Current Understanding of Cu-Exchanged Chabazite Molecular Sieves for Use as Commercial Diesel Engine DeNO(x) Catalysts, Top Catal, 56 (2013) 1441-1459.
[6] A.M. Beale, F. Gao, I. Lezcano-Gonzalez, C.H.F. Peden, J. Szanyi, Recent advances in automotive catalysis for NOx emission control by small-pore microporous materials, Chemical Society Reviews, 44 (2015) 7371-7405.
[7] F. Gao, C.H.F. Peden, Recent Progress in Atomic-Level Understanding of Cu/SSZ-13 Selective Catalytic Reduction Catalysts, Catalysts, 8 (2018) 140.
[8] F. Gao, J. Szanyi, On the hydrothermal stability of Cu/SSZ-13 SCR catalysts, Appl Catal a-Gen, 560 (2018) 185-194.
[9] C. Paolucci, J.R. Di Iorio, F.H. Ribeiro, R. Gounder, W.F. Schneider, Catalysis Science of NOx Selective Catalytic Reduction With Ammonia Over Cu-SSZ-13 and Cu-SAPO-34, Adv Catal, 59 (2016) 1-107.
[10] C.W. Andersen, M. Bremholm, P.N.R. Vennestrøm, A.B. Blichfeld, L.F. Lundegaard, B.B. Iversen, Location of Cu2+ in CHA zeolite investigated by X-ray diffraction using the Rietveld/maximum entropy method, IUCrJ, 1 (2014) 382-386.
[11] J. Song, Y.L. Wang, E.D. Walter, N.M. Washton, D.H. Mei, L. Kovarik, M.H. Engelhard, S. Prodinger, Y. Wang, C.H.F. Peden, F. Gao, Toward Rational Design of Cu/SSZ-13 Selective Catalytic Reduction Catalysts: Implications from Atomic-Level Understanding of Hydrothermal Stability, Acs Catal, 7 (2017) 8214-8227.
[12] R.Q. Zhang, J.S. McEwen, M. Kollar, F. Gao, Y.L. Wang, J. Szanyi, C.H.F. Peden, NO Chemisorption on Cu/SSZ-13: A Comparative Study from Infrared Spectroscopy and DFT Calculations, Acs Catal, 4 (2014) 4093-4105.
[13] C. Paolucci, A.A. Parekh, I. Khurana, J.R. Di Iorio, H. Li, J.D.A. Caballero, A.J. Shih, T. Anggara, W.N. Delgass, J.T. Miller, F.H. Ribeiro, R. Gounder, W.F. Schneider, Catalysis in a Cage: Condition-Dependent Speciation and Dynamics of Exchanged Cu Cations in SSZ-13 Zeolites, J Am Chem Soc, 138 (2016) 6028-6048.
[14] J.Y. Luo, F. Gao, K. Kamasamudram, N.W. Currier, C.H.F. Peden, A. Yezerets, New insights into Cu/SSZ-13 SCR catalyst acidity. Part I: Nature of acidic sites probed by NH3 titration, J Catal, 348 (2017) 291-299.
[15] A. Martini, E. Borfecchia, K.A. Lomachenko, I.A. Pankin, C. Negri, G. Berlier, P. Beato, H. Falsig, S. Bordiga, C. Lamberti, Composition-driven Cu-speciation and reducibility in Cu-CHA zeolite catalysts: a multivariate XAS/FTIR approach to complexity, Chem Sci, 8 (2017) 6836-6851.
[16] I. Lezcano-Gonzalez, U. Deka, H.E. van der Bij, P. Paalanen, B. Arstad, B.M. Weckhuysen, A.M. Beale, Chemical deactivation of Cu-SSZ-13 ammonia selective catalytic reduction (NH3-SCR) systems, Appl Catal B-Environ, 154 (2014) 339-349.
[17] F. Gao, Y.L. Wang, N.M. Washton, M. Kollar, J. Szanyi, C.H.F. Peden, Effects of Alkali and Alkaline Earth Cocations on the Activity and Hydrothermal Stability of Cu/SSZ-13 NH3-SCR Catalysts, Acs Catal, 5 (2015) 6780-6791.
[18] J.M. Fedeyko, H.Y. Chen, ZEOLITE CATALYST CONTAINING METALS, 2015.
[19] F. Gao, N.M. Washton, Y.L. Wang, M. Kollar, J. Szanyi, C.H.F. Peden, Effects of Si/Al ratio on Cu/SSZ-13 NH3-SCR catalysts: Implications for the active Cu species and the roles of Bronsted acidity, J Catal, 331 (2015) 25-38.

[20] S. Prodinger, M.A. Derewinski, Y.L. Wang, N.M. Washton, E.D. Walter, J. Szanyi, F. Gao, Y. Wang, C.H.F. Peden, Sub-micron Cu/SSZ-13: Synthesis and application as selective catalytic reduction (SCR) catalysts, Appl Catal B-Environ, 201 (2017) 461-469.
[21] F. Gao, E.D. Walter, M. Kollar, Y.L. Wang, J. Szanyi, C.H.F. Peden, Understanding ammonia selective catalytic reduction kinetics over Cu/SSZ-13 from motion of the Cu ions, J Catal, 319 (2014) 1-14.
[22] S.A. Bates, A.A. Verma, C. Paolucci, A.A. Parekh, T. Anggara, A. Yezerets, W.F. Schneider, J.T. Miller, W.N. Delgass, F.H. Ribeiro, Identification of the active Cu site in standard selective catalytic reduction with ammonia on Cu-SSZ-13, J Catal, 312 (2014) 87-97.
[23] F. Gao, E.D. Walter, E.M. Karp, J.Y. Luo, R.G. Tonkyn, J.H. Kwak, J. Szanyi, C.H.F. Peden, Structure-activity relationships in NH3-SCR over Cu-SSZ-13 as probed by reaction kinetics and EPR studies, J Catal, 300 (2013) 20-29.
[24] F. Gao, E.D. Walter, N.M. Washton, J. Szanyi, C.H.F. Peden, Synthesis and evaluation of Cu/SAPO-34 catalysts for NH3-SCR 2: Solid-state ion exchange and one-pot synthesis, Appl Catal B-Environ, 162 (2015) 501-514.
[25] P.N.R. Vennestrom, T.V.W. Janssens, A. Kustov, M. Grill, A. Puig-Molina, L.F. Lundegaard, R.R. Tiruvalam, P. Concepcion, A. Corma, Influence of lattice stability on hydrothermal deactivation of Cu-ZSM-5 and Cu-IM-5 zeolites for selective catalytic reduction of NOx by NH3, J Catal, 309 (2014) 477-490.
[26] A. Godiksen, F.N. Stappen, P.N.R. Vennestrom, F. Giordanino, S.B. Rasmussen, L.F. Lundegaard, S. Mossin, Coordination Environment of Copper Sites in Cu-CHA Zeolite Investigated by Electron Paramagnetic Resonance, J Phys Chem C, 118 (2014) 23126-23138.
[27] J.R. Di Iorio, R. Gounder, Controlling the Isolation and Pairing of Aluminum in Chabazite Zeolites Using Mixtures of Organic and Inorganic Structure-Directing Agents, Chem Mater, 28 (2016) 2236-2247.
[28] J.J. Xue, X.Q. Wang, G.S. Qi, J. Wang, M.Q. Shen, W. Li, Characterization of copper species over Cu/SAPO-34 in selective catalytic reduction of NOx with ammonia: Relationships between active Cu sites and de-NOx performance at low temperature, J Catal, 297 (2013) 56-64.
[29] J.H. Kwak, H.Y. Zhu, J.H. Lee, C.H.F. Peden, J. Szanyi, Two different cationic positions in Cu-SSZ-13?, Chem Commun, 48 (2012) 4758-4760.
[30] L.J. Xie, F.D. Liu, X.Y. Shi, F.S. Xiao, H. He, Effects of post-treatment method and Na co-cation on the hydrothermal stability of Cu-SSZ-13 catalyst for the selective catalytic reduction of NOx with NH3, Appl Catal B-Environ, 179 (2015) 206-212.
[31] F. Gao, D.H. Mei, Y.L. Wang, J. Szanyi, C.H.F. Peden, Selective Catalytic Reduction over Cu/SSZ-13: Linking Homo- and Heterogeneous Catalysis, J Am Chem Soc, 139 (2017) 4935-4942.
[32] C. Paolucci, I. Khurana, A.A. Parekh, S.C. Li, A.J. Shih, H. Li, J.R. Di Iorio, J.D. Albarracin-Caballero, A. Yezerets, J.T. Miller, W.N. Delgass, F.H. Ribeiro, W.F. Schneider, R. Gounder, Dynamic multinuclear sites formed by mobilized copper ions in NOx selective catalytic reduction, Science, 357 (2017) 898-903.
[33] I. Lezcano-Gonzalez, U. Deka, B. Arstad, A. Van Yperen-De Deyne, K. Hemelsoet, M. Waroquier, V. Van Speybroeck, B.M. Weckhuysen, A.M. Beale, Determining the storage, availability and reactivity of NH3 within Cu-Chabazite-based Ammonia Selective Catalytic Reduction systems, Phys Chem Chem Phys, 16 (2014) 1639-1650.

Table 1. BET surface area and t-plot pore volume of the Cu/H-SSZ-13 and Cu/Na-SSZ-13 catalysts.

Catalysts	**DG BET Surface Area (m^2/g)**	**DG Pore Volume (cm^3/g)**	**HTA BET Surface Area (m^2/g)**	**HTA Pore Volume (cm^3/g)**
1.0wt% Cu/H-SSZ-13	509	0.28	541	0.26
1.5wt% Cu/H-SSZ-13	541	0.28	541	0.26
2.0wt% Cu/H-SSZ-13	554	0.28	542	0.25
2.5wt% Cu/H-SSZ-13	541	0.27	546	0.26
3.0wt% Cu/H-SSZ-13	557	0.28	506	0.24
3.5wt% Cu/H-SSZ-13	546	0.28	538	0.25
4.0wt% Cu/H-SSZ-13	538	0.27	458	0.22
4.5wt% Cu/H-SSZ-13	534	0.27	401	0.19
5.0wt% Cu/H-SSZ-13	493	0.27	291	0.13
1.0wt% Cu/Na-SSZ-13	545	0.26	527	0.25
1.5wt% Cu/Na-SSZ-13	544	0.27	528	0.25
2.0wt% Cu/Na-SSZ-13	549	0.27	448	0.21
2.5wt% Cu/Na-SSZ-13	530	0.26	327	0.15
3.0wt% Cu/Na-SSZ-13	527	0.26	316	0.15
3.5wt% Cu/Na-SSZ-13	507	0.25	386	0.19
4.0wt% Cu/Na-SSZ-13	505	0.25	79	0.03

Table 2. Apparent activation energy and turn-over rate summary of Cu/H-SSZ-13 and Cu/Na-SSZ-13 catalysts. Reaction feed contains 360 ppm NO_x (containing ~20 ppm NO_2), 360 ppm NH_3, 14% O_2, 2.5% H_2O balanced with N_2 at a GHSV of 667,000 h^{-1}. Temperatures were varied from 180 – 100 °C.

Catalyst	DG		HTA	
	E_a (kJ/mol)	**TOR at 180 °C (10^{-3}/s)**	**E_a (kJ/mol)**	**TOR at 180 °C (10^{-3}/s)**
1.0wt% Cu/H-SSZ-13	42	3.3	43	2.0
2.0wt% Cu/H-SSZ-13	68	4.0	58	3.6
3.0wt% Cu/H-SSZ-13	78	6.0	47	3.8
4.0wt% Cu/H-SSZ-13	63	5.2	68	4.1
1.0wt% Cu/Na-SSZ-13	52	7.2	40	4.9
2.0wt% Cu/Na-SSZ-13	73	12.1	52	8.4
3.0wt% Cu/Na-SSZ-13	65	15.2	62	5.3
4.0wt% Cu/Na-SSZ-13	66	10.3	63	1.8

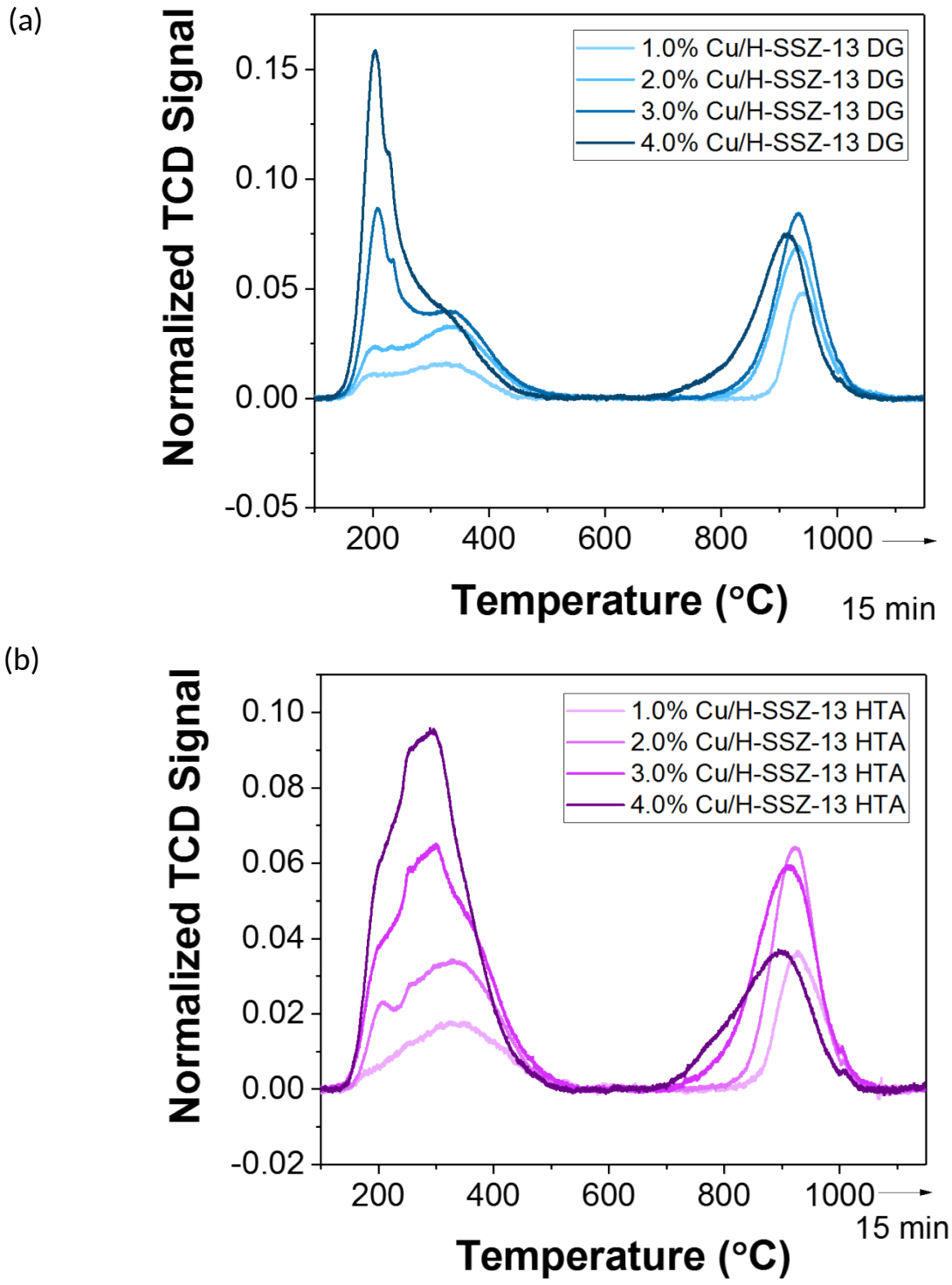

Figure 1. H_2-TPR profiles of selected (a) degreened and (b) hydrothermally aged Cu/H-SSZ-13 catalysts. Flow rate 50 ml/min 10% H_2/Ar, ramping rate 10 °C/min.

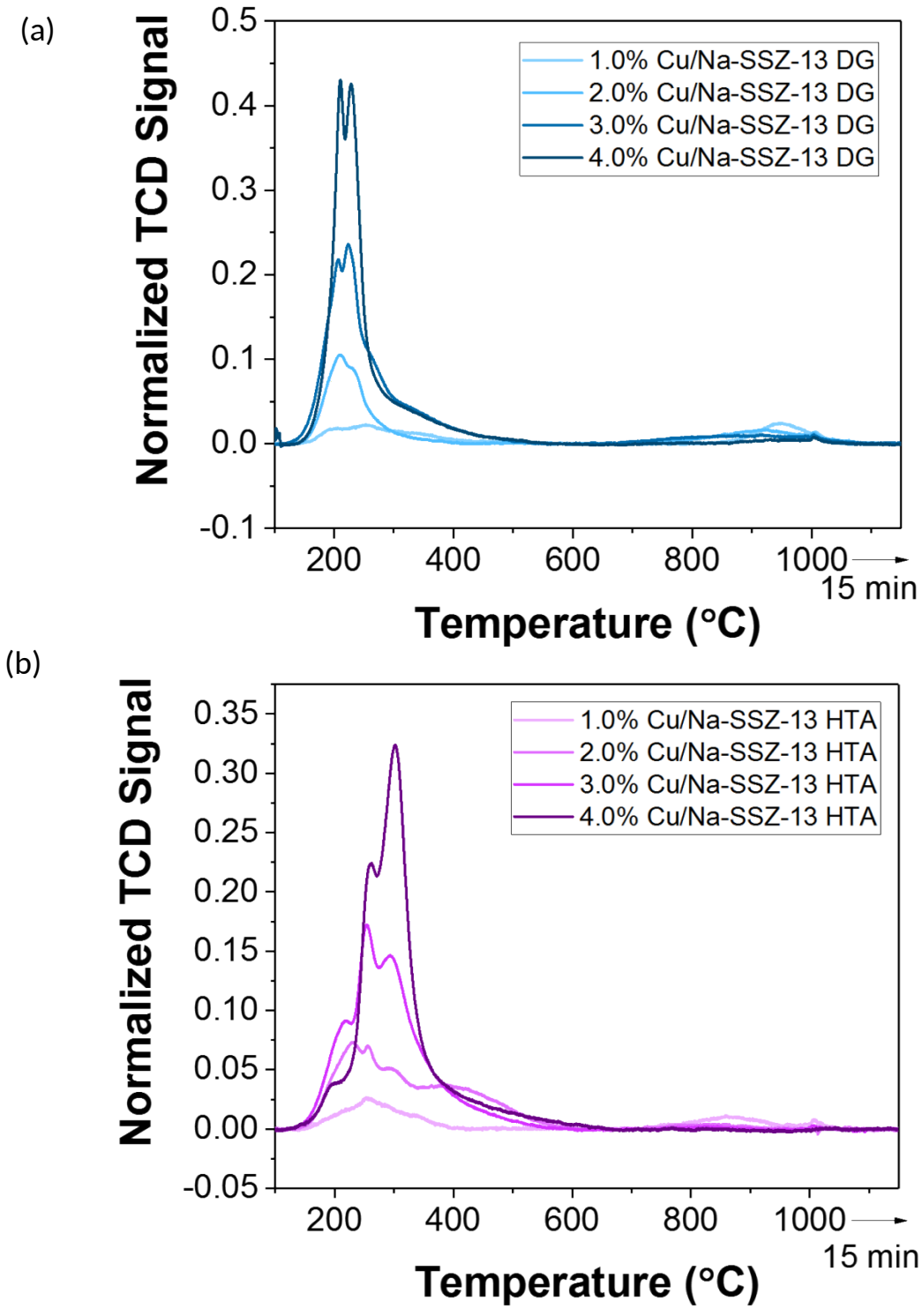

Figure 2. H_2-TPR profiles of selected (a) degreened and (b) hydrothermally aged Cu/Na-SSZ-13 catalysts. Flow rate 50 ml/min 10% H_2/Ar, ramping rate 10 °C/min.

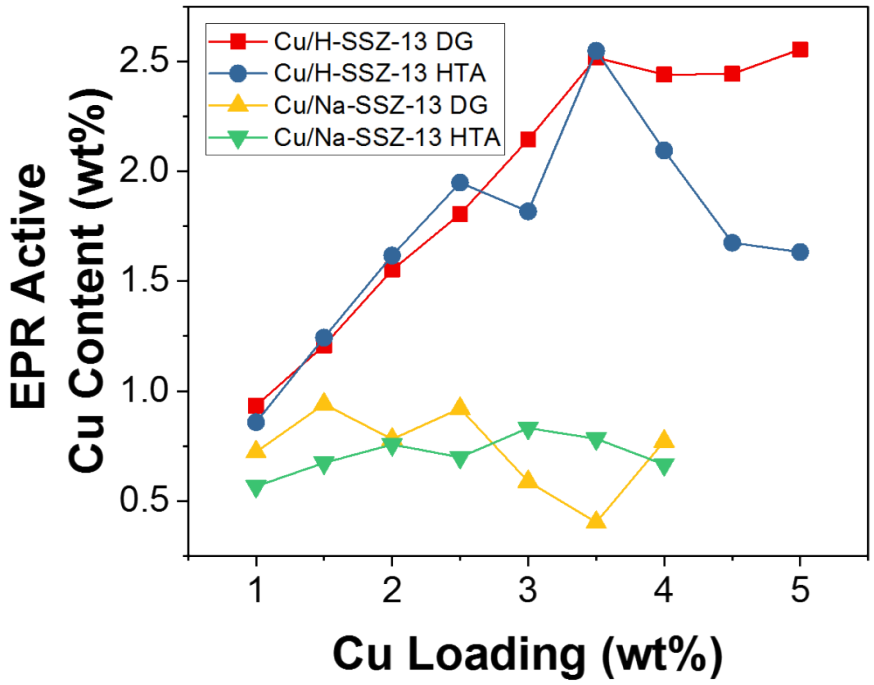

Figure 3. EPR active Cu(II) contents of DG and HTA Cu/H-SSZ-13 and Cu/Na-SSZ-13 catalysts with different Cu loadings. Measurement temperature 125 K.

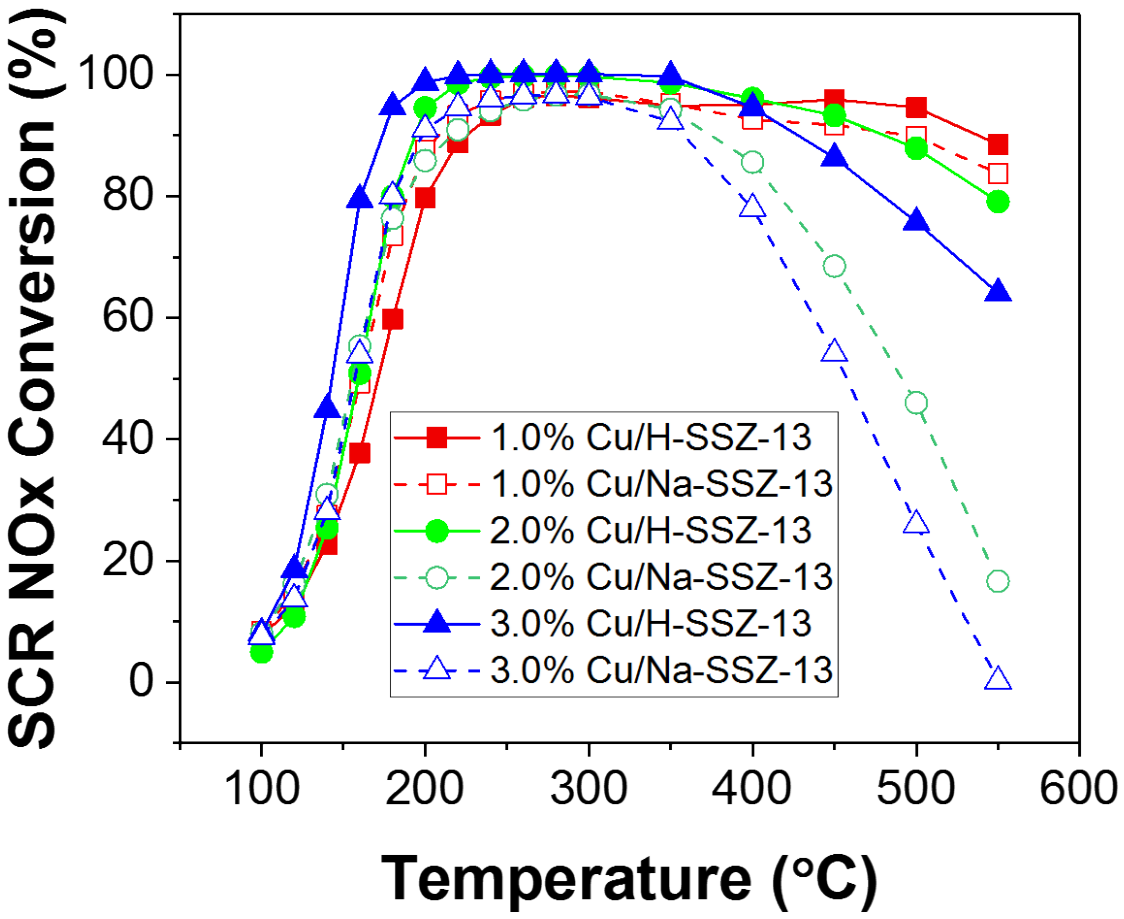

Figure 4. NO_x conversion as a function of temperature during standard SCR for selected DG Cu/H-SSZ-13 and Cu/Na-SSZ-13 catalysts. Reactant feed contains 360 ppm NO_x (containing ~20 ppm NO_2), 360 ppm NH_3, 14% O_2, 2.5% H_2O balanced with N_2 at a GHSV of 100,000 h^{-1}.

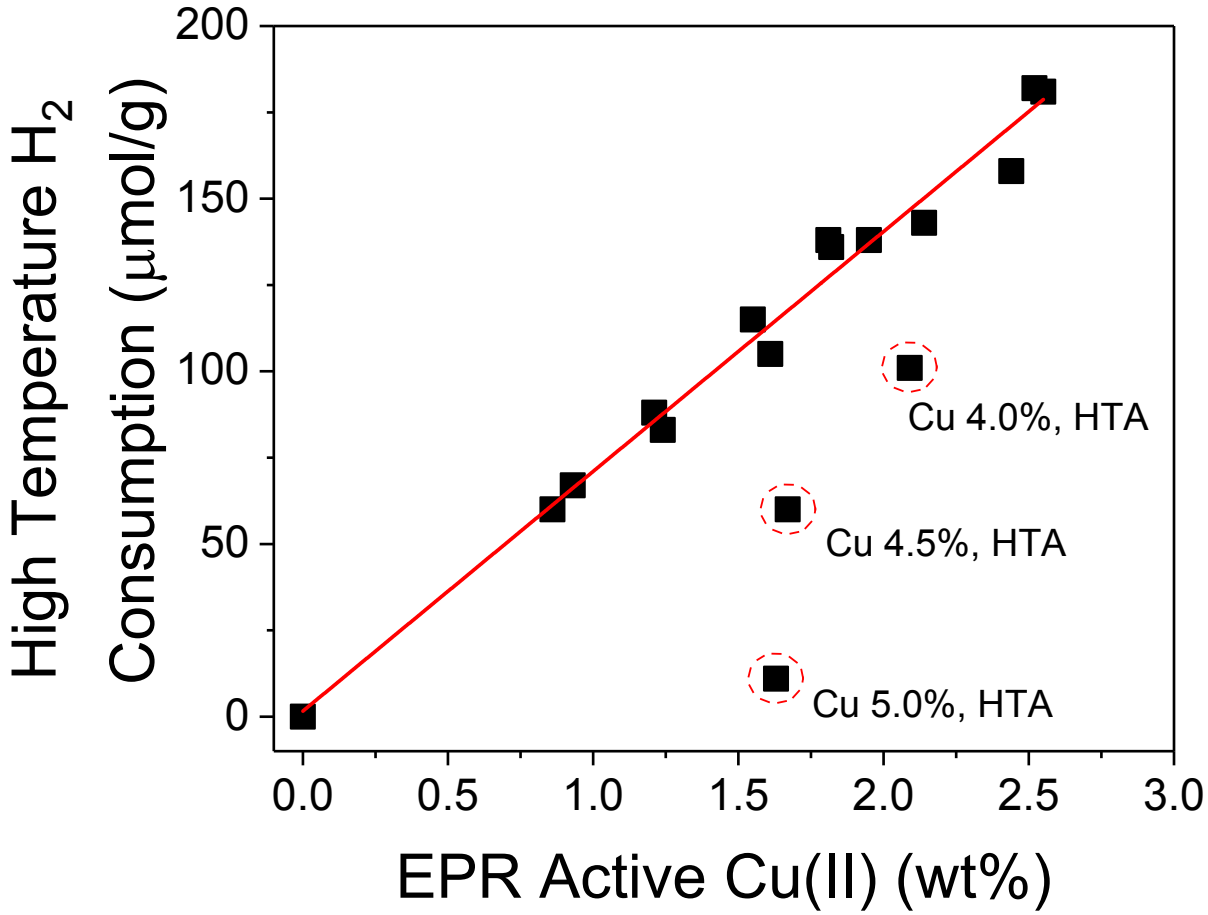

Figure 5. Concentrations of EPR active Cu(II)-ions versus high-temperature (> 700 °C) H_2 consumption in H_2-TPR for DG and HTA Cu/H-SSZ-13 samples. Note that an excellent linear correlation (R-square > 0.98) exists except for HTA samples at high Cu loadings (marked with dashed cycles).

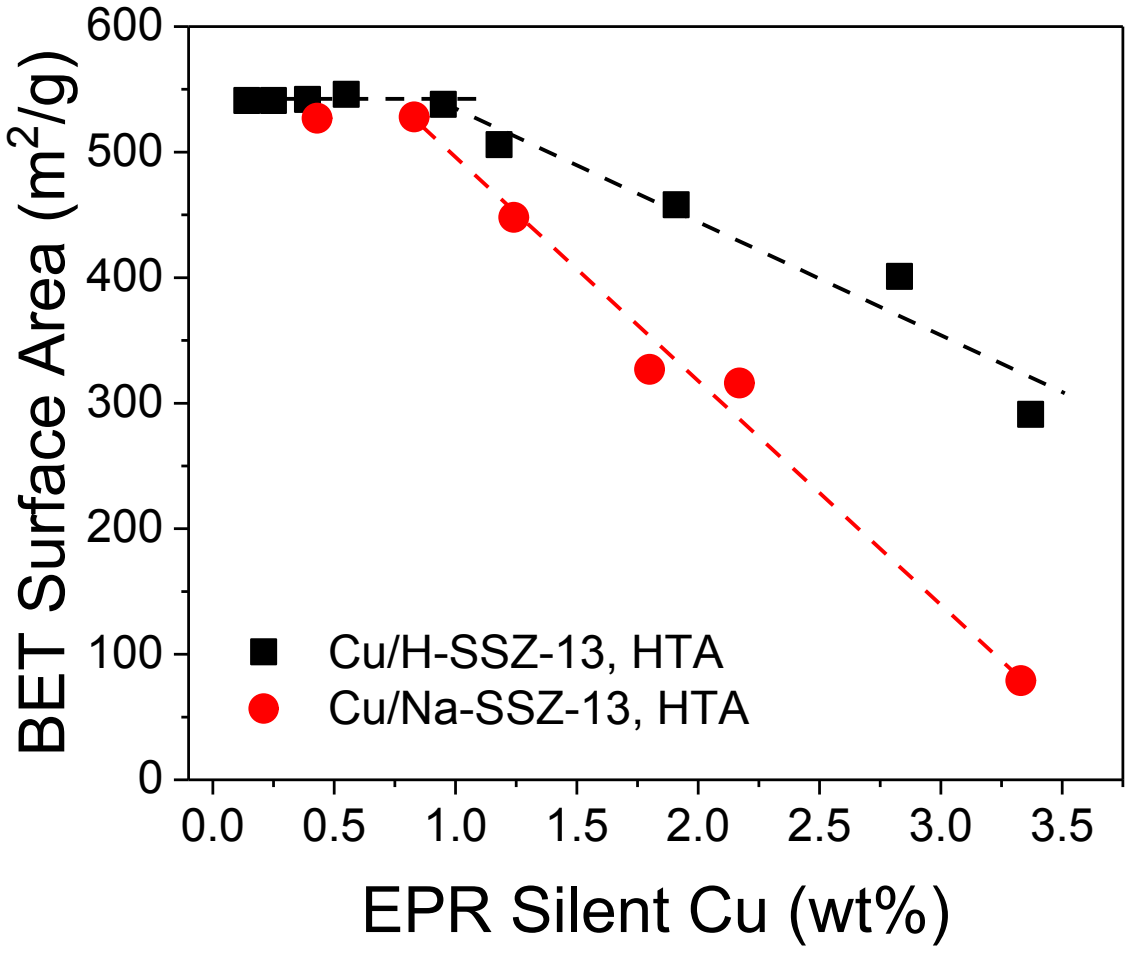

Figure 6. BET surface area as a function of EPR silent Cu contents for the HTA Cu/H-SSZ-13 and Cu/Na-SSZ-13 samples. Dashed lines serve as visual guides to the eye.

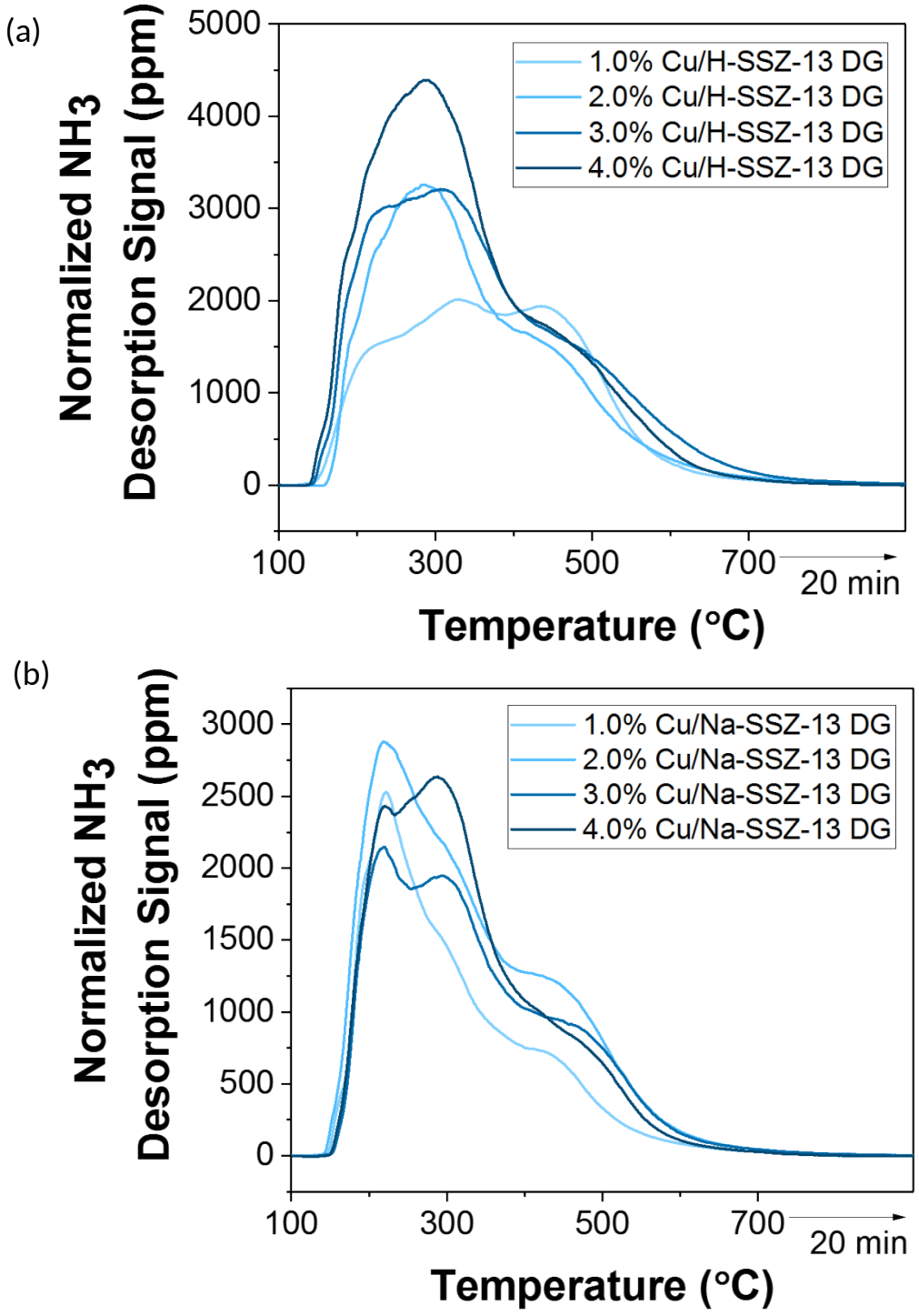

Figure 7. NH_3-TPD results on selected DG (a) Cu/H-SSZ-13 and (b) Cu/Na-SSZ-13 catalysts. NH_3 adsorption and purging were performed at 100 °C, ramping rate was 10 °C/min, N_2 gas flow rate 300 ml/min.

Supporting Information

Influences of Na^+ co-cation on the structure and performance of Cu/SSZ-13 selective catalytic reduction catalysts

Yanran Cui, Yilin Wang, Eric D. Walter, János Szanyi, Yong Wang, Feng Gao*

Institute for Integrated Catalysis, Pacific Northwest National Laboratory, P.O. Box 999, Richland, WA 99354, United States

*Corresponding author – email address: feng.gao@pnnl.gov (F. Gao).

Table S1. H_2-TPR Quantification results for Cu/H-SSZ-13 catalysts.

Cu Loading (wt%)	Treatment	Low Temperature Region H_2 Consumption (μmol/g)	High Temperature Region H_2 Consumption (μmol/g)
1.0	DG	52	67
	HTA	62	60
1.5	DG	93	88
	HTA	98	83
2.0	DG	118	115
	HTA	124	105
2.5	DG	166	138
	HTA	167	138
3.0	DG	198	143
	HTA	212	136
3.5	DG	236	182
	HTA	225	181
4.0	DG	266	158
	HTA	278	101
4.5	DG	332	139
	HTA	434	60
5.0	DG	474	103
	HTA	567	11

Table S2. H_2-TPR Quantification results for Cu/Na-SSZ-13 catalysts.

Cu Loading (wt%)	Treatment	Low Temperature Region H_2 Consumption (μmol/g)	High Temperature Region H_2 Consumption (μmol/g)
1.0	DG	65	43
	HTA	53	29
1.5	DG	94	56
	HTA	164	26
2.0	DG	148	53
	HTA	248	9
2.5	DG	327	11
	HTA	323	4
3.0	DG	401	47
	HTA	398	2
3.5	DG	455	3
	HTA	446	10
4.0	DG	514	12
	HTA	536	1

In the H_2-TPR measurements of the Cu/H-SSZ-13 and Cu/Na-SSZ-13 samples, the reducing gas was 10% H_2/Ar with a flow rate of 50 ml/min, and the ramping rate was set at 10 °C/min. Peak areas of the two temperature regimes (low temperature, ≤ 500 °C, and high temperature, ≥ 700 °C) were quantified using CuO reduction as the standard. Differences of the low- and high-temperature H_2 consumption represent the amounts of CuO_x and $CuAl_2O_4$ moieties in the catalysts, which are reduced to Cu^0 exclusively below 500 °C.

(a)

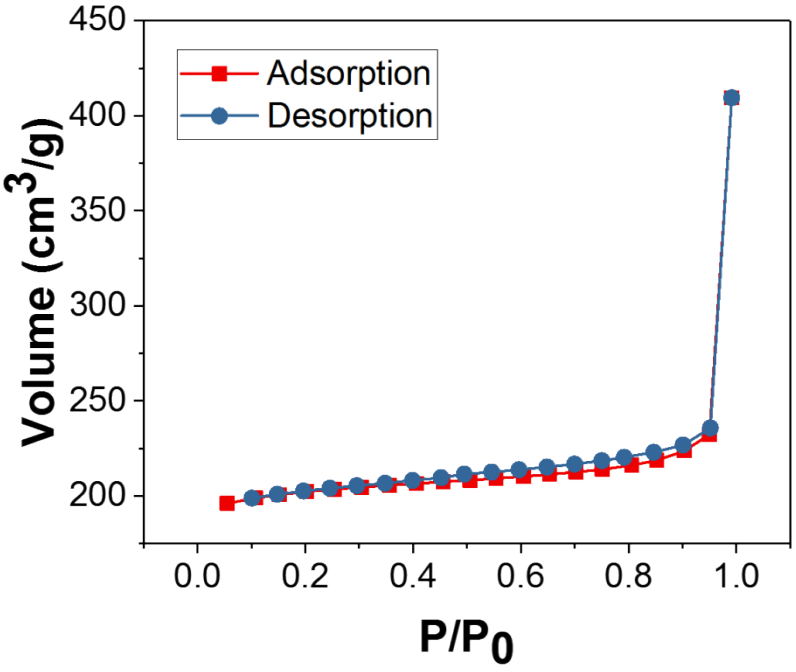

(b)

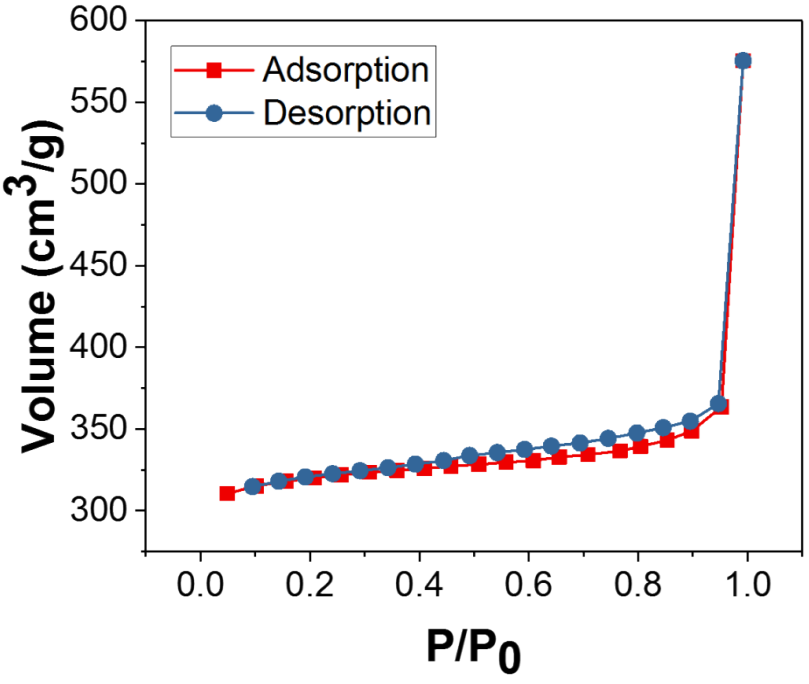

Figure S1. N_2 adsorption/desorption isotherms of the freshly prepared supports (a) NH_4-SSZ-13, (b) Na-SSZ-13.

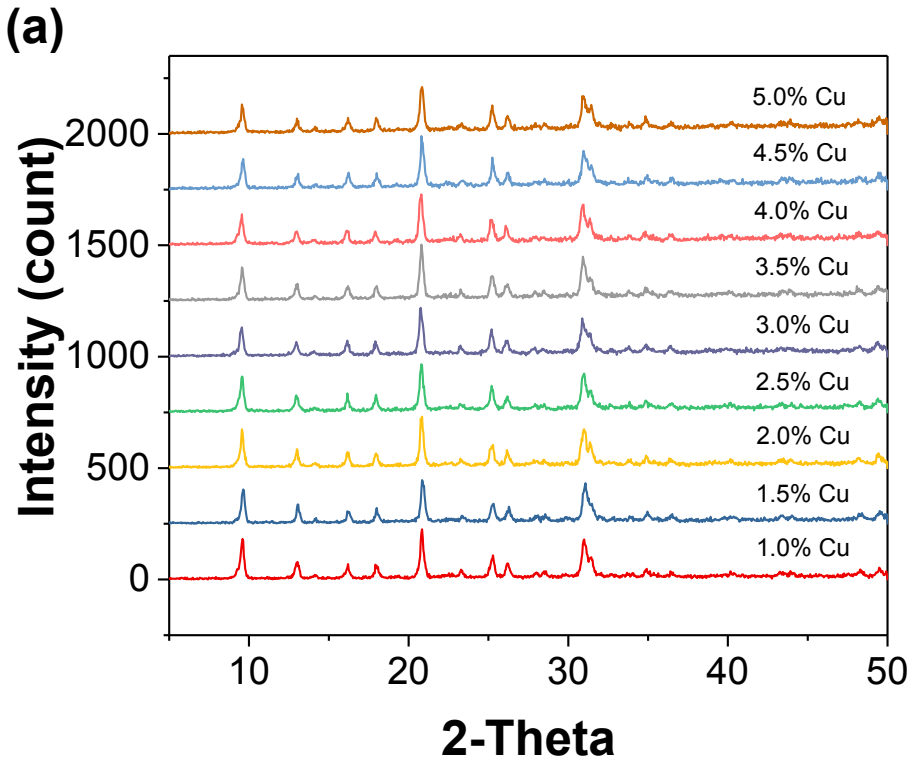
(a)
Intensity (count)
2000
1500
1000
500
0
5.0% Cu
4.5% Cu
4.0% Cu
3.5% Cu
3.0% Cu
2.5% Cu
2.0% Cu
1.5% Cu
1.0% Cu
10
20
30
40
50
2-Theta

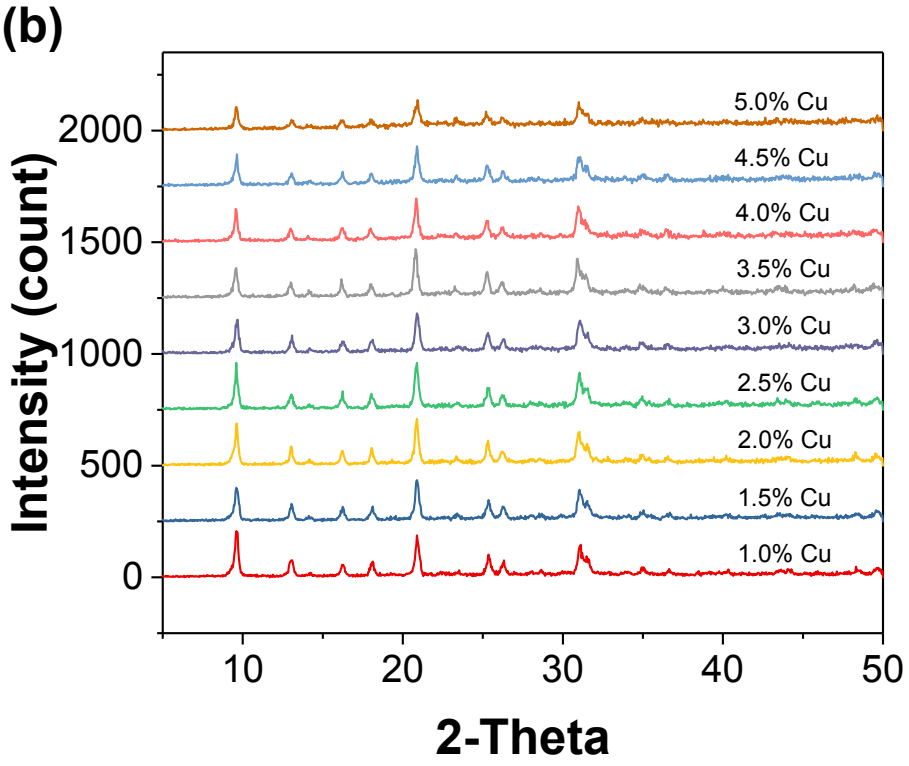
(b)
Intensity (count)
2000
1500
1000
500
0
5.0% Cu
4.5% Cu
4.0% Cu
3.5% Cu
3.0% Cu
2.5% Cu
2.0% Cu
1.5% Cu
1.0% Cu
10
20
30
40
50
2-Theta

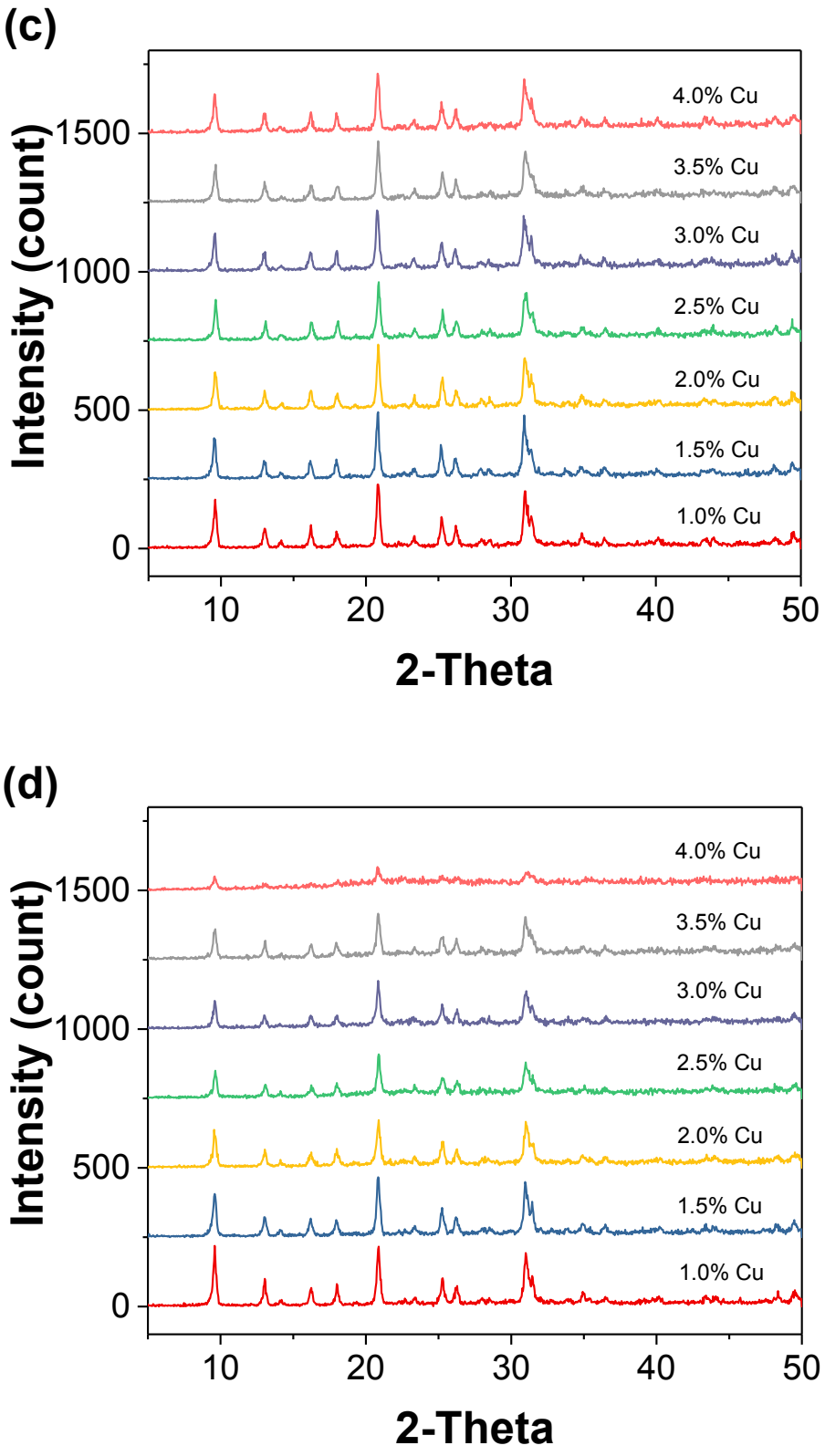

Figure S2. XRD patterns of the Cu catalysts: (a) Cu/H-SSZ-13 DG; (b) Cu/H-SSZ-13 HTA; (c) Cu/Na-SSZ-13 DG; (d) Cu/Na-SSZ-13 HTA.

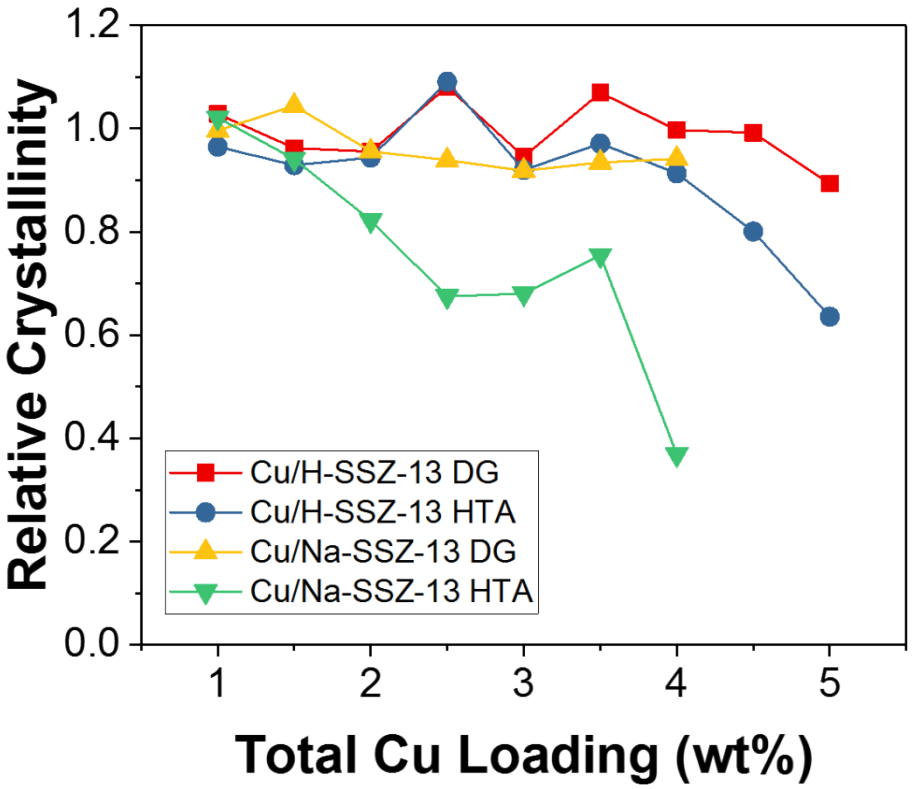

Figure S3. Relative crystallinities of the Cu/H-SSZ-13 and Cu/Na-SSZ-13 catalysts after DG and HTA treatments.

To calculate relatively crystallinities, five strongest diffraction peaks for each sample were summed, and the relative crystallinity was calculated based on the equation below:

$$\text{Relative Crystallinity} = \frac{Peak\ Intensity\ of\ the\ treated\ catalysts}{Peak\ Intensity\ of\ the\ fresh\ catalysts}$$

From the results, the degreening treatment does not alter the crystal structures irrespective to Cu loading for both series of samples. However the more severe hydrothermal aging at 800 °C causes clear decrease in crystallinity for some samples. In the absence of Na^+, this decrease only occurs on relatively high Cu loaded samples. In the presence of Na^+, relative crystallinity decrease even occurs at low Cu loadings. For the 4.0 wt% Cu/Na-SSZ-13 catalyst, the crystal structure was severely destroyed after hydrothermal ageing Changes in crystallinity are fully consistent with the BET surface area and pore volume analyses shown by **Table 1**.

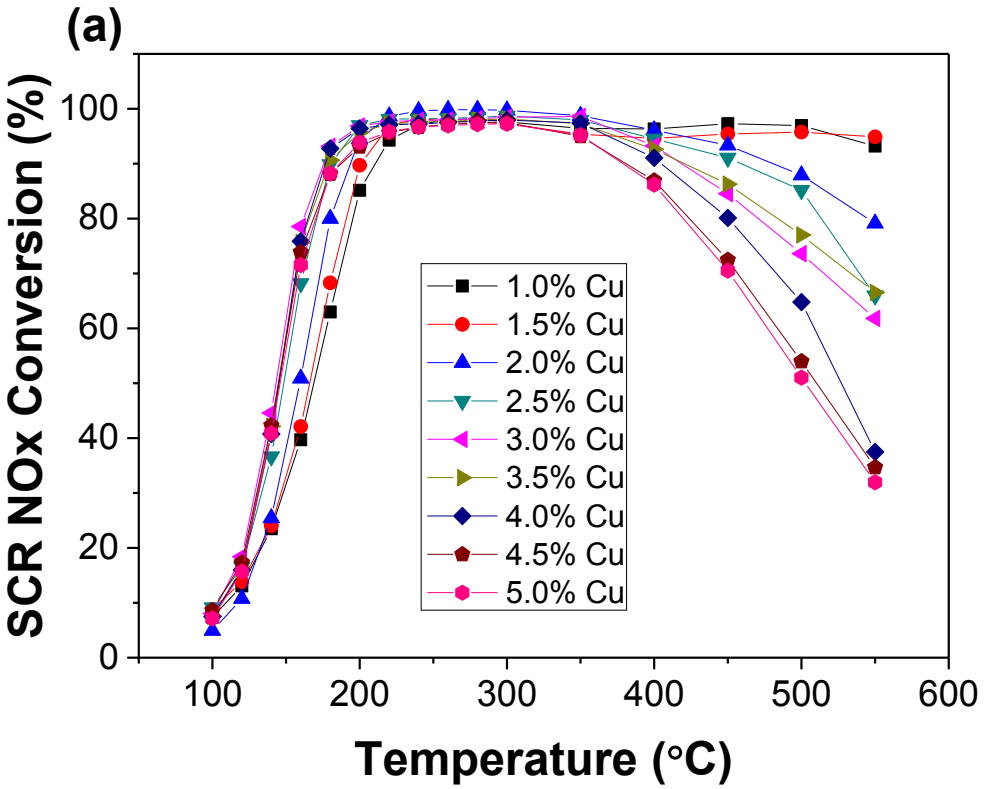
(a)
SCR NOx Conversion (%)
Temperature (°C)
1.0% Cu
1.5% Cu
2.0% Cu
2.5% Cu
3.0% Cu
3.5% Cu
4.0% Cu
4.5% Cu
5.0% Cu

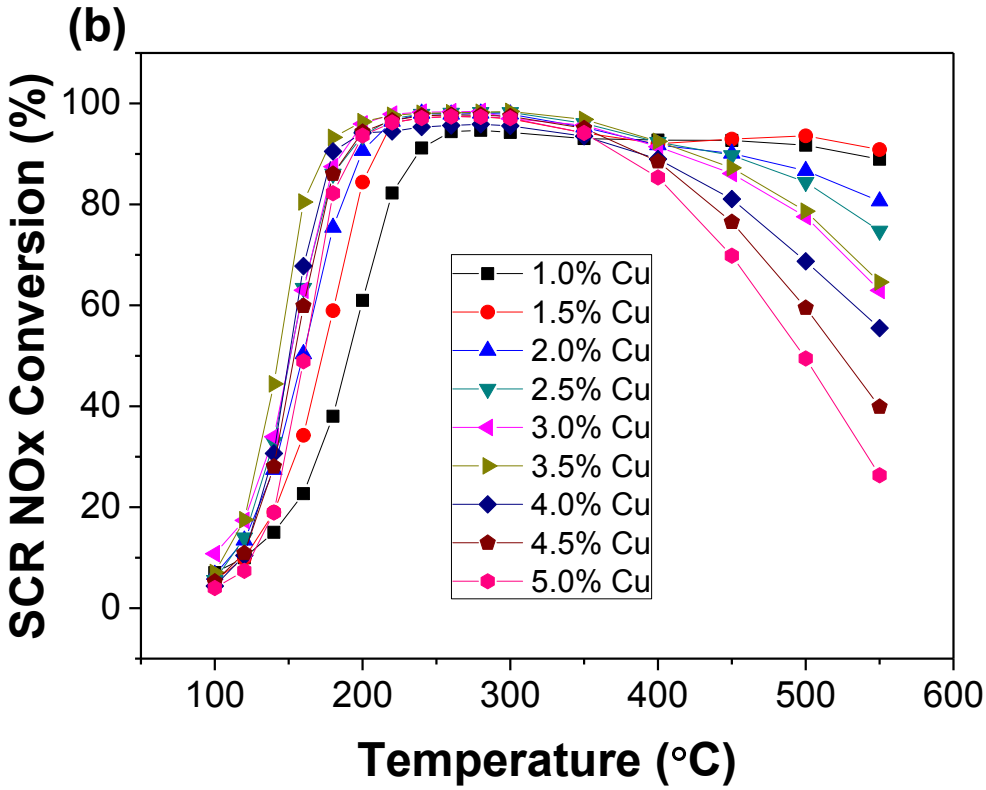
(b)
SCR NOx Conversion (%)
Temperature (°C)
1.0% Cu
1.5% Cu
2.0% Cu
2.5% Cu
3.0% Cu
3.5% Cu
4.0% Cu
4.5% Cu
5.0% Cu

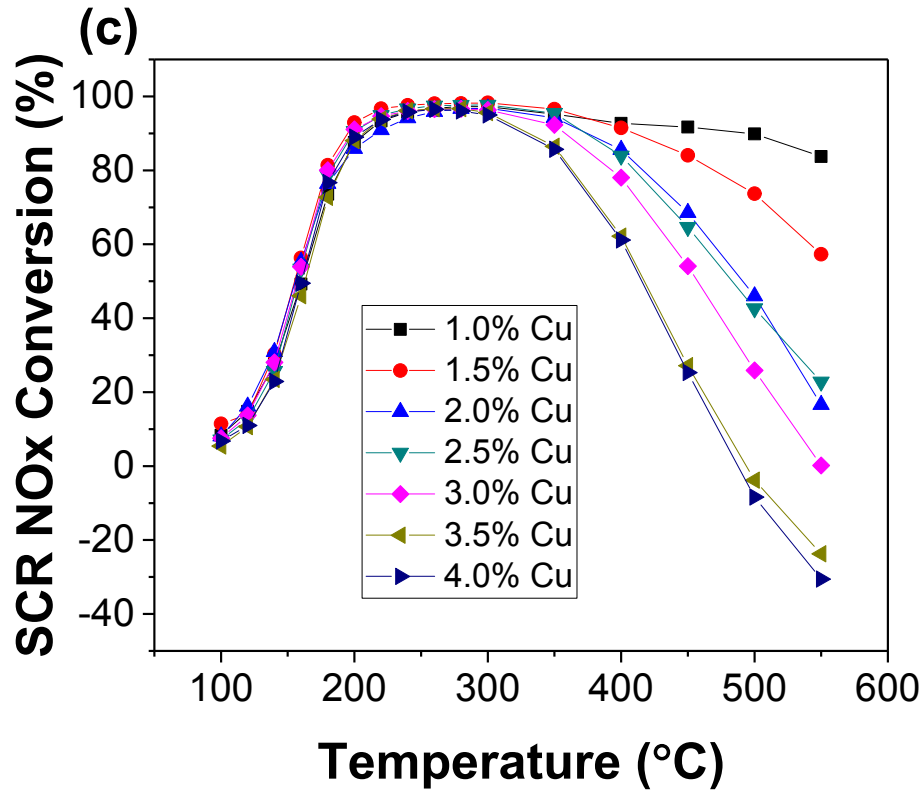

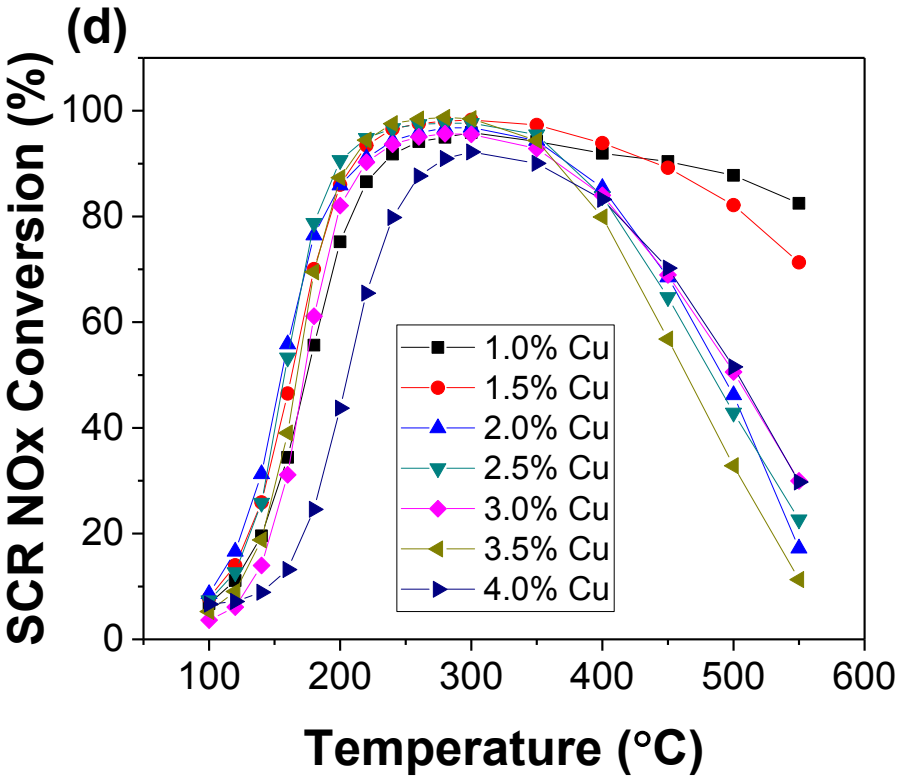

Figure S4. NOx conversion as a function of temperature during standard SCR for (a) DG Cu/H-SSZ-13, (b) HTA Cu/H-SSZ-13, (c) DG Cu/Na-SSZ-13, and (d) HTA Cu/Na-SSZ-13 catalysts. Reactant feed contains 360 ppm NO_x (containing ~20 ppm NO_2), 360 ppm NH_3, 14% O_2, 2.5% H_2O balanced with N_2 at a GHSV of 100,000 h^{-1}.

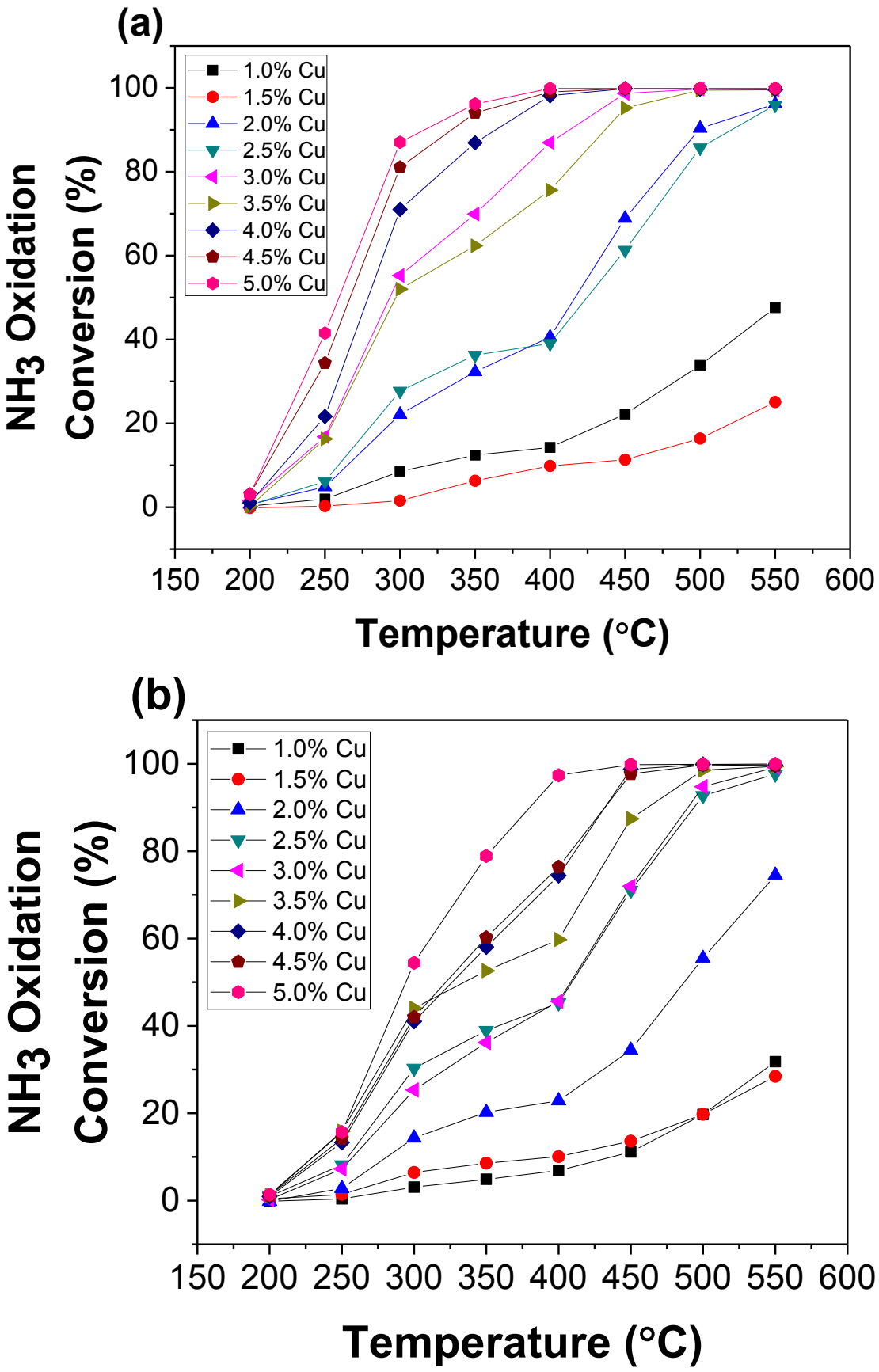
(a)
1.0% Cu
1.5% Cu
2.0% Cu
2.5% Cu
3.0% Cu
3.5% Cu
4.0% Cu
4.5% Cu
5.0% Cu
NH3 Oxidation Conversion (%)
0
20
40
60
80
100
150 200 250 300 350 400 450 500 550 600
Temperature (°C)
(b)
1.0% Cu
1.5% Cu
2.0% Cu
2.5% Cu
3.0% Cu
3.5% Cu
4.0% Cu
4.5% Cu
5.0% Cu
NH3 Oxidation Conversion (%)
0
20
40
60
80
100
150 200 250 300 350 400 450 500 550 600
Temperature (°C)

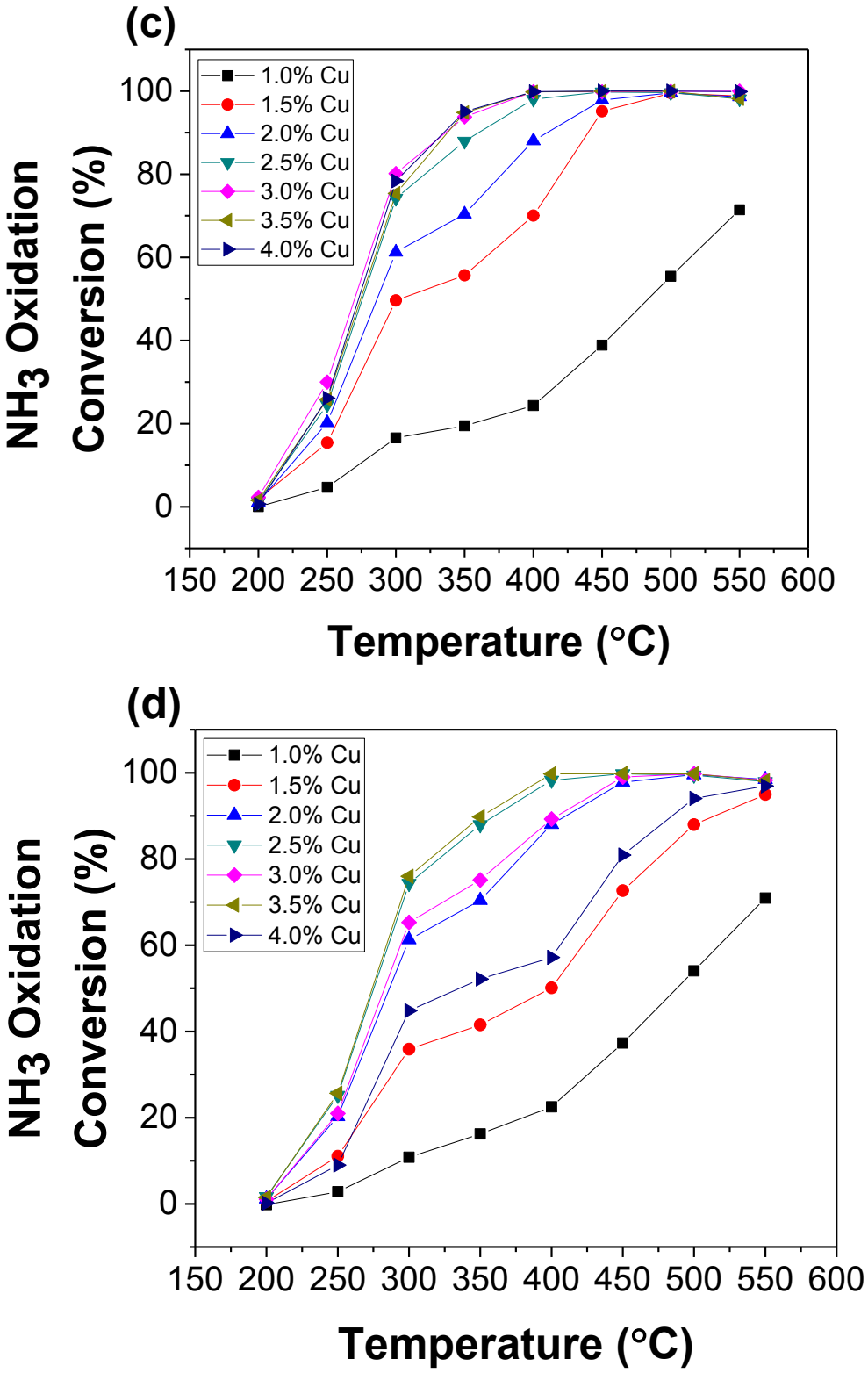

Figure S5. NH_3 conversion as a function of temperature during NH_3 oxidation reaction for (a) DG Cu/H-SSZ-13, (b) HTA Cu/H-SSZ-13, (c) DG Cu/Na-SSZ-13, and (d) HTA Cu/Na-SSZ-13 catalysts.. Reactant feed contains 380 ppm NH_3, 14% O_2, 2.5% H_2O balanced with N_2 at a GHSV of 100,000 h^{-1}.

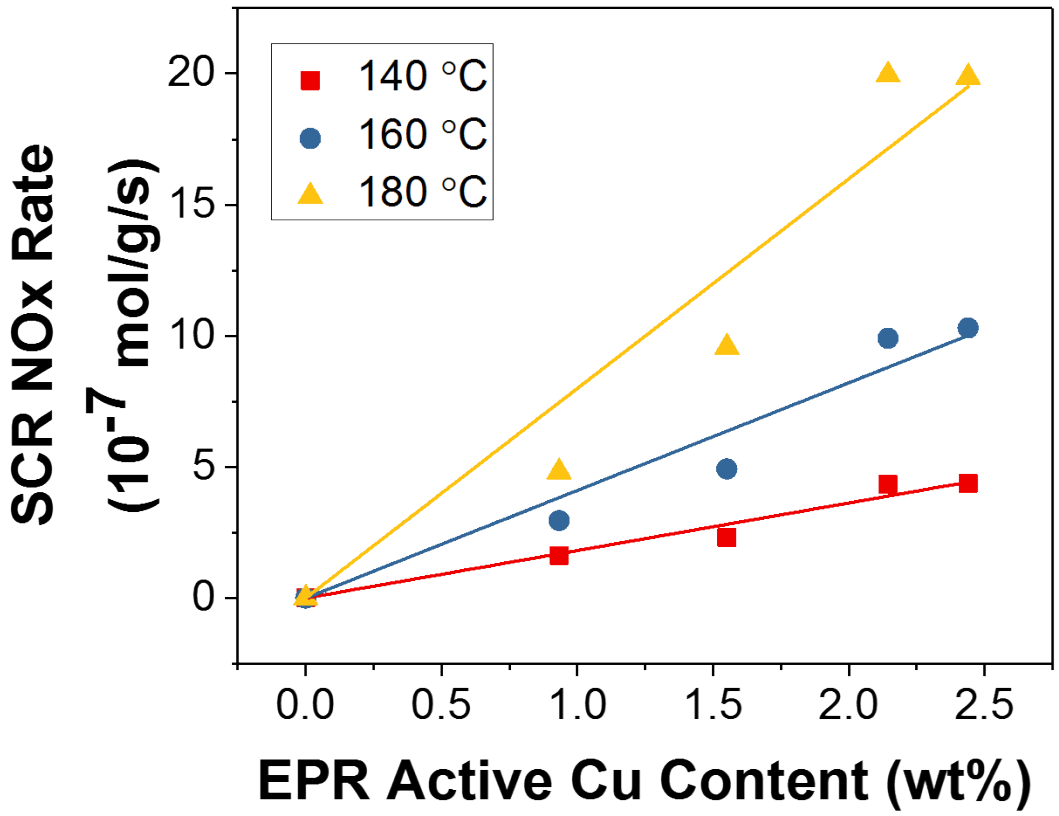

Figure S6. Koros-Nowak test of the Cu/H-SSZ-13 DG catalysts at different temperatures. The NO_x conversion rates are normalized to catalyst weights.

(a)

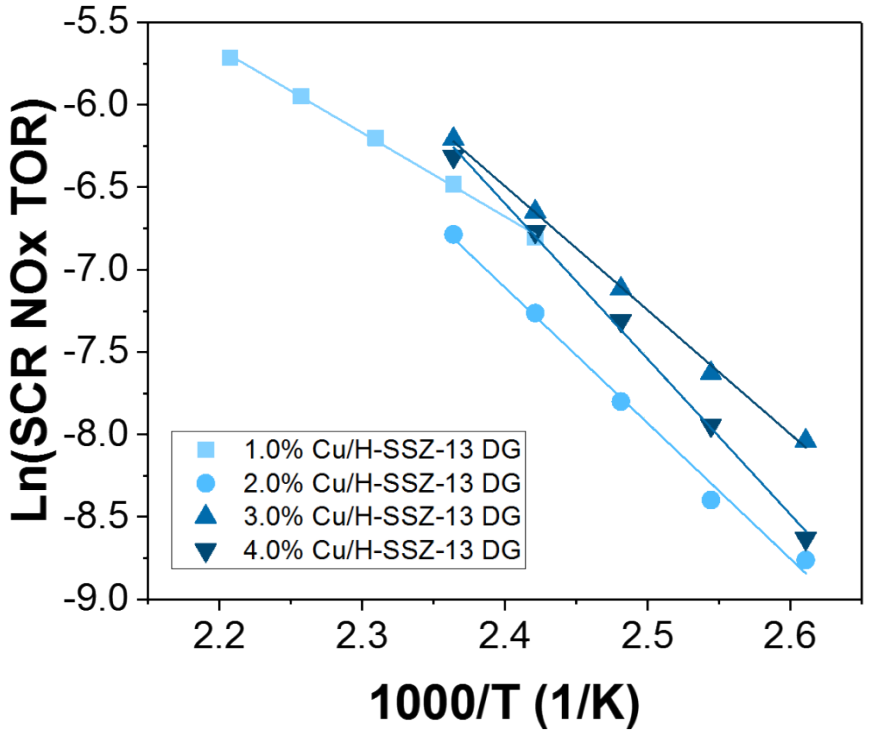
-5.5
-6.0
-6.5
-7.0
-7.5
-8.0
-8.5
-9.0
Ln(SCR NOx TOR)
2.2
2.3
2.4
2.5
2.6
1000/T (1/K)
1.0% Cu/H-SSZ-13 DG
2.0% Cu/H-SSZ-13 DG
3.0% Cu/H-SSZ-13 DG
4.0% Cu/H-SSZ-13 DG

(b)

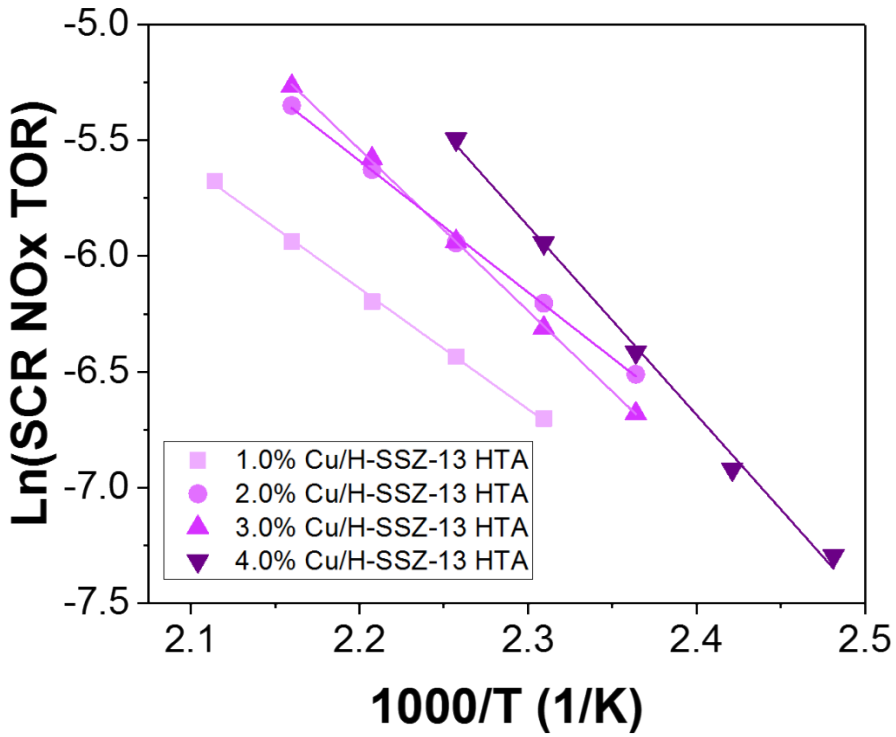
-5.0
-5.5
-6.0
-6.5
-7.0
-7.5
Ln(SCR NOx TOR)
2.1
2.2
2.3
2.4
2.5
1000/T (1/K)
1.0% Cu/H-SSZ-13 HTA
2.0% Cu/H-SSZ-13 HTA
3.0% Cu/H-SSZ-13 HTA
4.0% Cu/H-SSZ-13 HTA

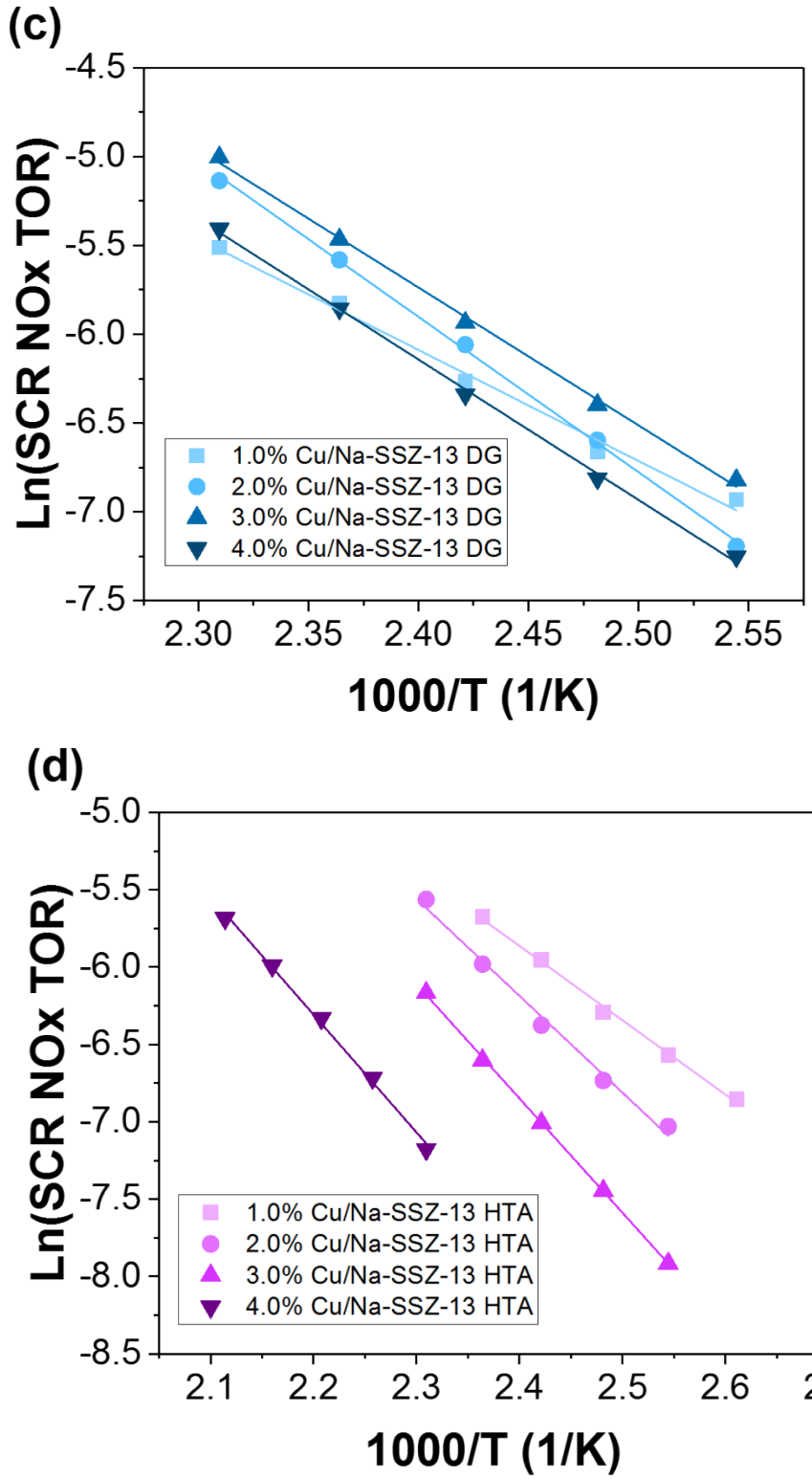

Figure S7. Arrhenius plot of the (a) Cu/H-SSZ-13 DG, (b) Cu/H-SSZ-13 HTA, (c) Cu/Na-SSZ-13 DG and (d) Cu/Na-SSZ-13 catalysts. Reactant feed contains 360 ppm NOx (containing ~20 ppm NO_2), 360 ppm NH_3, 14% O_2, 2.5% H_2O balanced with N_2 at a GHSV of 667,000 h^{-1}.

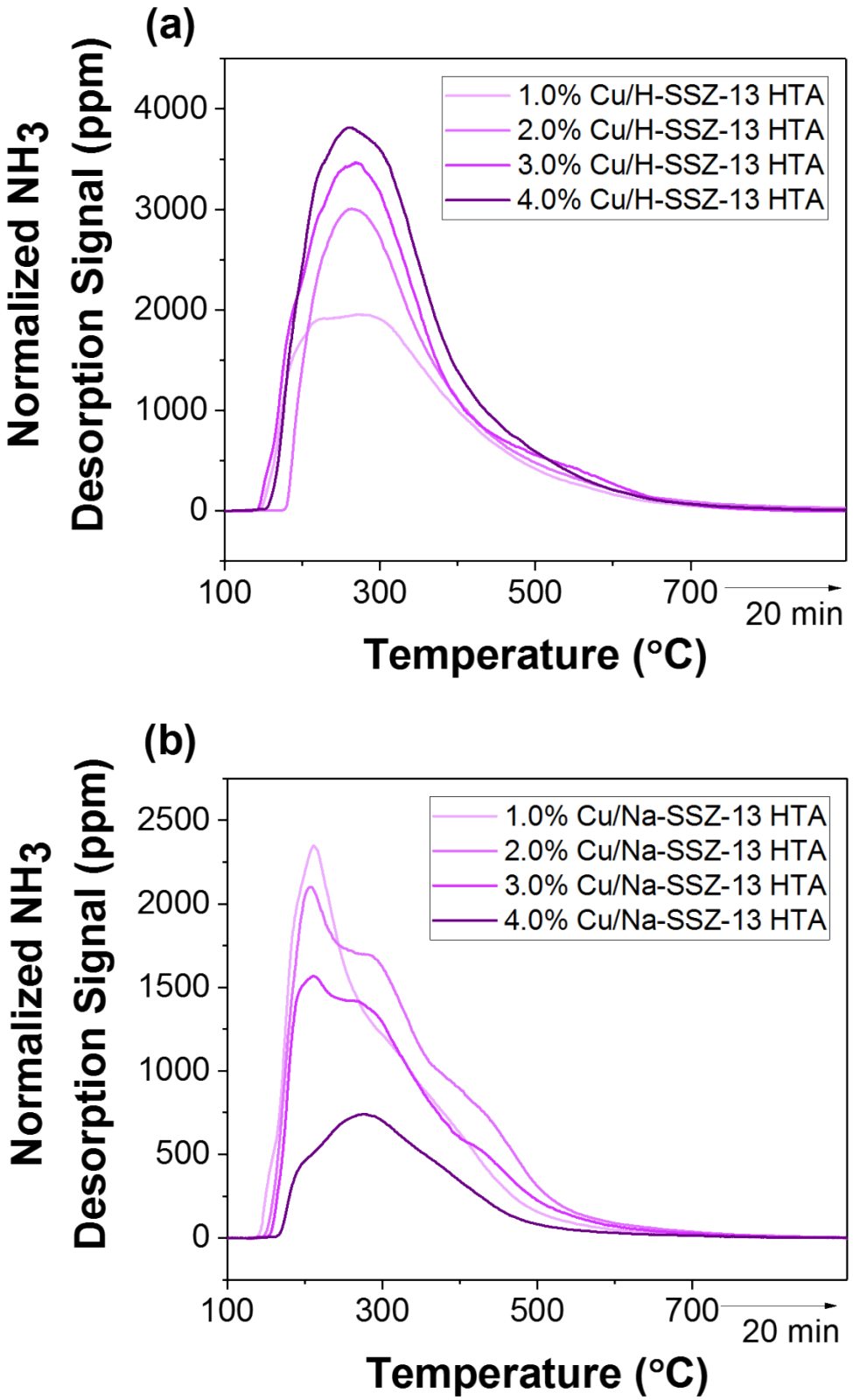

Figure S8. NH_3-TPD results on selected (a) Cu/H-SSZ-13 and (b) Cu/Na-SSZ-13 HTA catalysts. NH_3 adsorption and purging were performed at 100 °C, ramping rate was 10 °C/min, N_2 gas flow rate 300 ml/min.

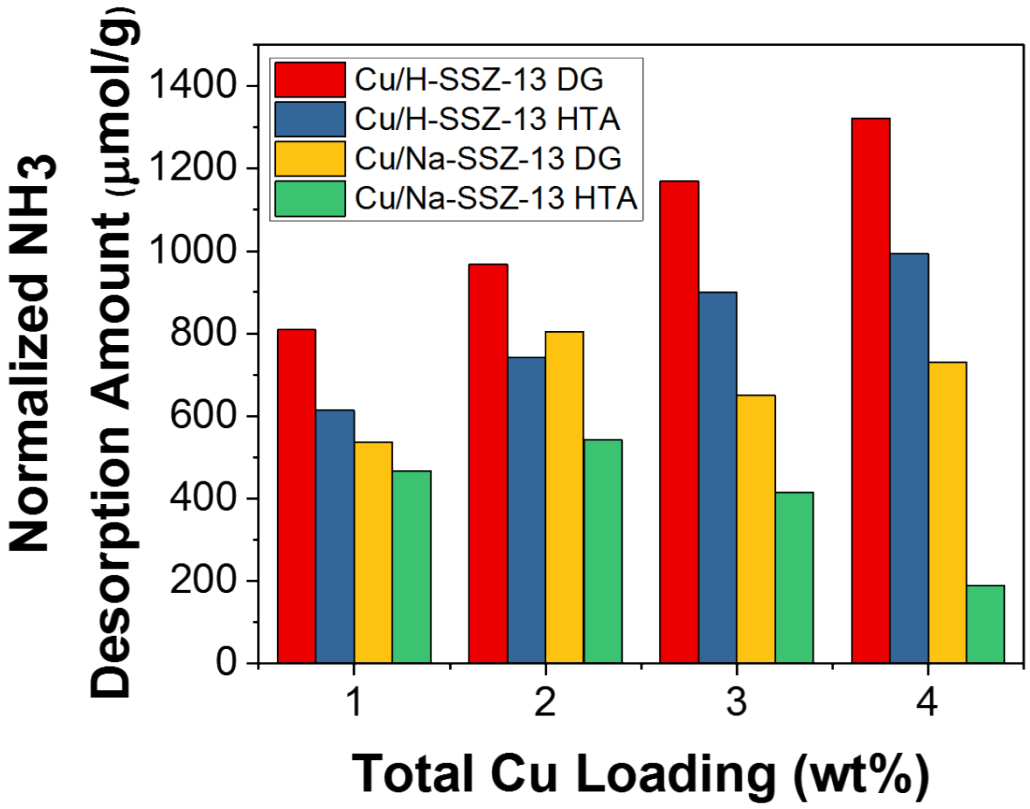

Figure S9. NH_3-TPD quantification results for Cu/H-SSZ-13 and Cu/Na-SSZ-13 catalysts with degreening and hydrothermal ageing treatments. Ramping rate was 10 °C/min, and N_2 gas flow was 300 ml/min.